Reinforcement Learning with Gaussian Processes for Unmanned Aerial Vehicle Navigation

Nahush Gondhalekar

Thesis submitted to the Faculty of the
Virginia Polytechnic Institute and State University
in partial fulfillment of the requirements for the degree of

Master of Science
in
Computer Engineering

Pratap Tokekar, Chair
Haibo Zeng
A. Lynn Abbott

June 23, 2017
Blacksburg, Virginia

Keywords: Reinforcement Learning, Gaussian Processes, Unmanned Aerial Vehicle Navigation

Reinforcement Learning with Gaussian Processes for Unmanned Aerial Vehicle Navigation

Nahush Gondhalekar

We present the problem of studying reinforcement learning (RL) for unmanned aerial vehicle (UAV) navigation with as few real world samples as possible. A naive implementation suffers from curse of dimensionality in large continuous state spaces. Gaussian Processes(GPs) exploit the spatial correlation to approximate state-action transition dynamics in large state spaces. By incorporating GPs in naive Q-learning we achieve better performance in lesser number of samples. The illustrations are performed using simulations with an aerial robot. Further, we present a Multi-Fidelity Reinforcement Learning (MFRL) algorithm that leverages Gaussian Processes (GP) to learn the optimal policy in a real world environment.In MFRL framework, an agent uses multiple simulators of the real environment to perform actions. With multiple levels of fidelity in a simulator chain, the number of samples used in successively higher simulators can be reduced. This is illustrated with the help of simulations. One of the promising yet fairly unexplored applications of learning autonomous navigation for aerial robots is in Structural Inspection.

This work has been funded by the Center for Unmanned Aircraft Systems (C-UAS), a National Science Foundation-sponsored industry/university cooperative research center (I/UCRC) under NSF Award No. IIP-1161036 along with significant contributions from C-UAS industry members.

Dedication

To Dad and Maa.

Acknowledgments

First and foremost, I would like to express my gratitude towards my advisor, Dr. Pratap Tokekar. Thank you very much for the constant support and motivation. This wouldn't be possible without your encouragement. My sincere acknowledgment for believing in me. I am looking forward to have a continued association and keep learning new things and hoping to collaborate in the future. I could not have asked for a better advisor.

A sincere thank you to my co-author Varun Suryan for his contribution to this thesis. I am thankful to the National Science Foundation for the financial support NSF Award No. IIP-1161036. A special thanks to Dr. Matt Hebdon and his team for the collaboration in the bridge inspection project which is the work presented in Chapter 5.

Robotics Algorithms and Autonomous Systems lab (`http://www.raas.ece.vt.edu/`) has been home for over 18 months; thanks to all the team members who made this time enjoyable. Thank you Ashish Budhiraja, Kevin Yu, Aravind, Lifeng Zhou, Yoonchang Sung, Varun Suryan and Zhongshun Zhang for all the help and fun times at the outdoor experiments. It has been a wonderful one and a half years and I am very proud to be a part of this research group.

I would be short of words to fully express my thanks towards one person who has been an essential part of my life at Virginia Tech. Thank you so much Harsh Patel who has been more of a brother than a friend and has been with me through all the ups and downs and is more than a family to me. Thanks to all the friends in Virginia Tech for the fun times. Thank you Shefali Gundecha who has always been there to support me despite being in a different timezone. Thanks for being there when I needed it the most.

I'd like to express my sincere thanks to the Mccomas Gym and the War Memorial Gym at Virginia Tech which have been my meditation centers and have helped me through the stressful times.

Last but certainly not the least, I cannot describe how thankful I am towards my family. My mother's confidence in me and her endless support has kept me going for these two years. Thank you to my mother Sudha Gondhalekar for being just a phone call away. A special thanks to my dad Ramesh Gondhalekar who's been watching over me from heaven for the past 5 years and I know he would continue to do so.

Contents

List of Figures

Chapter 1

Introduction

With increasing popularity of mobile robots and challenges in their autonomous navigation, a variety of problems can be phrased as the ones of *Reinforcement Learning* (RL). Reinforcement learning in the robotics domain differs considerably from most well-studied reinforcement learning benchmark problems. Problems in robotics are often high-dimensional and are best represented by a continuous state-action space. The true state is not always observable and noise-free. Sometimes, greatly different states may look very similar. It is often essential to know the state of the robot in the environment which gives information with uncertainty. It can be difficult to obtain real-world experience since it is often tedious to obtain and hard to reproduce. In order to learn a particular task at hand within reasonable time, approximations of the environment and system dynamics are used through simulations. However, no matter how costly the real-world experience is, it wholly cannot be replaced by simulations. Smallest of the modeling errors can accumulate to cause a different behavior in the real world.

In particular, obtaining negative samples may require the robot to collide or fail which is undesirable. Hence, it is desirable to minimize the number of real world samples required for learning optimal paths or desired tasks. With a better understanding of reinforcement learning framework for robotics, we may be able to answer fundamental questions such as: What skills are needed to be learned by the robot achieve a particular task? How can we reduce the number of real world samples by optimally building the simulators? How to use approximations in order to learn the desired skill within an acceptable time?

In this thesis we study these questions for the specific application of Unmanned Aerial Vehicle (UAV). Before introducing the particular problems, we will discuss the challenges in navigation for specific motivating applications.

1.1 Motivation and applications to general scenarios

This work is motivated by the growing interest in using small UAVs for infrastructure and environmental monitoring. UAVs equipped high resolution cameras are being used for bridge inspection (28, 8), penstock inspection (36, 6), and yield estimation in farms (14, 4). In order for these systems to be successfully deployed, it is crucial that UAVs are able to plan and navigate autonomously in narrow, confined spaces while withstanding large wind disturbances. A controller that is not robust to these disturbances may cause catastrophic failures. Designing custom controllers for UAVs in every new situation is a tedious task and not practical as it requires constant human supervision (22, 2). Instead, reinforcement learning (RL) can provide a general solution.

Navigating safely through a previously-unseen environment is of paramount importance as colliding with obstacles can be catastrophic for a flying object. As shown in Figure 1.1, the quadrotor needs to navigate through the narrow corridor flying close to the surfaces for visual inspection. The main challenge here is to design the control robust enough to perform such tasks when the external localization signals are not available. The next section discusses a few of the main challenges in performing structural inspection using UAVs.

Figure 1.1: Quadrotor navigating through a confined space without GPS signal. Images collected during field trial reported in Chapter 5.

1.1.1 Challenges

When a UAV needs to inspect a bridge from inside or when it tries to fly near the structures or around the bridge pillars, GPS signal is either not available or not reliable. In order to be able to autonomously navigate such areas, the UAV must be equipped with an ability to fly close to the surfaces using on-board sensors such as laser range-finders.

A flight control system with conventional methods where the designer needs to be aware of the dynamics of the vehicle and environment increases the development time. If some modifications are made to the vehicle later, most of the controller tuning may be needed to be

redone from scratch. Reinforcement learning algorithms provide a number of characteristics which could partly address dynamic environments and dynamics changes: RL can control an agent when a model of the environment is unavailable; RL can control an agent without an existing programmed system; and RL can compensate for changes in the environment as they are encountered since the agent continuously *explores* and *learns*.

One of several immediate questions is: how does the *learning* occur? In many control systems, stability is critically important. Having a *trial and error* way of experimentation may result in a crash which is unacceptable. Trying out experiments in real world is expensive. Development of simulators in order to maximize the performance minimizing the real world costs is crucial. The main contributions of this thesis in development of some RL algorithms centered around UAV navigation reducing real world samples is discussed next.

1.2 Contributions

A Multi-Fidelity Reinforcement Learning (MFRL) algorithm that leverages Gaussian Processes (GPs) to learn the optimal policy in a real world environment is presented in this thesis. In the MFRL framework, an agent uses multiple simulators of the real environment to perform actions. With multiple levels of fidelity in a simulator chain, the number of samples used while learning in successively higher simulators can be reduced. The main contribution of this thesis is to show how we can use GP regression with MFRL to approximate the state-action transition dynamics in large state spaces. GPs exploit the spatial correlation in the transition function for agents that are physical grounded (e.g., a robot). By incorporating GP in the MFRL framework, we achieve further reduction in the number of samples used as we move up the simulator chain. We examine the performance with the help of simulations for navigation with an aerial robot.

We also present an implementation of an *End to End GPQ algorithm* based on a recent work on batch off policy RL with a GP (10, 0). The feedback from the laser sensors is utilized by the learning algorithm in order to *learn* a particular *skill*. The algorithm uses GP regression to learn the Q values associated with the skill of obstacle avoidance in a dynamic environment. The algorithm is testes in a python simulator with a simple kinematic robot model. The learned Q values are transferred to the Gazebo Robot Simulator and an actual quadrotor as the highest fidelity simulator.

1.3 Organization of the Thesis

The thesis is organized in five chapters.

In Chapter 2, we present a review of the fundamental concepts and background of sequential decision making, reinforcement learning and Gaussian processes.

In Chapter 3, we present the End-to-End GPQ algorithm which forms the basis of the Multi-Fidelity Reinforcement Learning presented in the next chapter.

Chapter 4 covers Multi-Fidelity Reinforcement Learning with Gaussian Processes. This framework helps to reduce the number of real world samples.

Chapter 5 discusses the motivating application of bridge inspection for the algorithms presented in the thesis along with preliminary field experiments.

We conclude the thesis with an overview of the main contributions and discussions of future work. All the software corresponding to this thesis is available online on github. The source code for the Gazebo Robot Simulator implementation of the GPQ algorithm: `https://github.com/nahush8/wall_follower`. The python based basic kinematic simulator: `https://github.com/nahush8/obstacle_avoidance`, The GP-MFRL algorithm: `https://github.com/raaslab/gp_gazebo`.

Chapter 2

Motivating Application: Bridge Inspection

2.1 Background

UAVs can be truly disruptive technology for inspecting civil infrastructure. They are capable of giving engineers eyes in the hardest to reach places, without the need for expensive access vehicles or potentially dangerous rigging or ladders or harnesses. A recent paper (33, 3) discusses the application of UAVs for visual inspection and damage detection of civil structures. The quality of pictures and videos taken by the UAV strongly depends on various factors viz. lighting conditions, distance from the structure, vehicle motion which is influenced by environmental factors. It is very important for the UAVs to be equipped with sophisticated control algorithms and sensors to be able to provide reliable data which can be conclusively used for inspection and analysis of damage.

2.1.1 Conventional Inspection of Bridges

Figure 5.1 shows typical inspection units like under-bridge units or truck cranes. Inspection units are in most cases expensive custom products. Often, specially trained staff, like industrial climbers, can get access to special parts of the structure but they can rarely evaluate what influences detected damages have on these structures. Therefore, they can only take photos or videos of the concerned part of the structure, which must be analyzed by civil engineers off-line.

It can be dangerous to use such large truck cranes. Figure 5.2 shows an unfortunate incident where the inspection truck tipped over causing a life threating situation for the people involved.

(a) Truck Crane (b) Under Bridge Inspection unit

Figure 2.1: Conventional inspection units for Bridge Inspection: (left, Bridge Inspection platform with a truck crane.), A-30 Hi-Rail Under Bridge Units (right, N.E. Bridge Contractors Inc.)

(?, ?)

Figure 2.2: Bridgeriggers' Aspen A-75 under-bridge inspection crane overturns on Sakonnet River Bridge in Rhode Island, August 30, 2016.

(?, ?)

UAVs often have following advantages in comparison to the conventional bridge-inspection methods.

- UAVs only need an operator on the ground for controlling the flight and the camera. A more advanced scenario includes *autonomous* UAVs navigating around the structures while collecting the required data such as pictures and videos.
- UAVs can be used in high-risk situations without endangering human lives. Situations like Figure 5.2 could be avoided.
- UAVs are capable of fast real time data acquisition and the storage of all the relevant flight data. They can process data on-board and adaptively collect information.
- Overall, they often turn out to be lower in costs compared to the large custom inspection units. In particular, expensive insurance for human operators will be avoided.

Despite the obvious advantages, UAVs have some essential limitations.

- Due to the small payload capacity of the UAVs, only small format and light digital compact cameras can be used for visual inspection.
- The smaller payload also affects the battery size leading to shorter flight times.
- Due to unexpected flight situations or due to unreliable GPS-signal strength, a change from the autonomous flight mode into a manual mode can be required which demands a skillful pilot to override the control.
- Currently, UAVs are not equipped with effective collision avoidance systems.

2.2 Preliminary Experiments

We performed experiments in order to analyze the limitations and challenges of performing autonomous navigation of UAVs around bridges. We performed several manual flights of a UAV on the Smart Road Bridge (the tallest state-maintained bridge in Virginia). Another set of field experiments were performed at the George Coleman Memorial Bridge, Yorktown, VA. The goal of the experiments was to capture visuals of the inside as well as the outside of the bridge for analysis of the structure and to analyze challenges in order to improve the system for fully autonomous flights.

2.2.1 System Setup

DJI model F450 (1,) was used as shown in the Figure 5.3. The UAV is equipped with sensors, controller and an on-board computer.

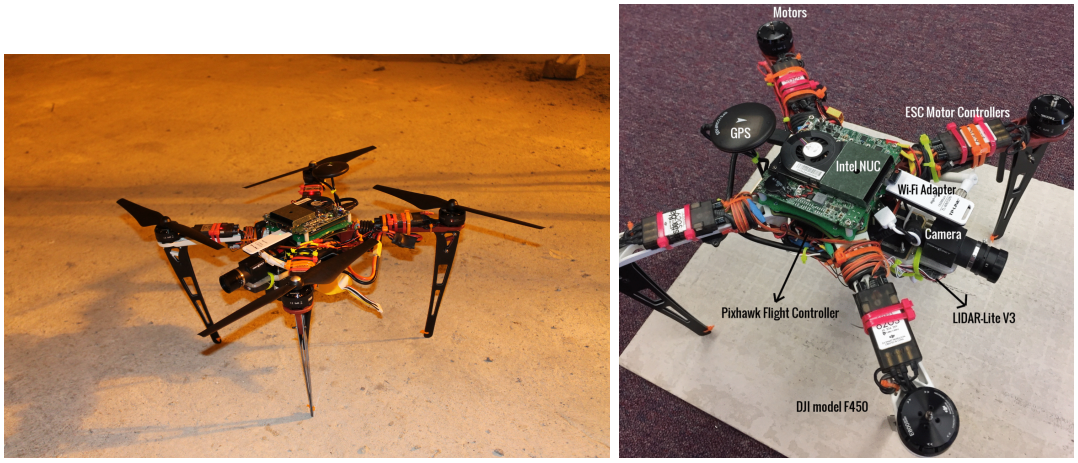

Figure 2.3: The UAV used for the experiments.

- **Camera**: The camera used to capture the visuals is a global shutter (2,) as shown in Figure 5.5. The resolution of the images is 1600 × 1200 and can capture images upto 59 FPS.

Figure 2.4: Flea3 2.0 MP Color USB3 Vision. (e2v EV76C5706F)

- **Intel NUC**: Intel NUC5I7RYH Mini PC NUC Kit as shown in Figure 5.6.

Figure 2.5: Intel NUC NUC5I7RYH

Specifications are as follows:

- 5th Generation Intel Core *i*7-5557U processor
- Intel Iris Graphics 6100
- Mini HDMI & Mini Display Port
- Internal support for M.2 SSD card & SATA3 for 2.5“ HDD/SSD

- **Pixhawk-Flight Controller**: Pixhawk is an independent, open-hardware project which mainly aims at providing high-end autopilot hardware to the academic, hobby and industrial communities at low costs as shown in Figure 5.7. The Pixhawk autopilot module runs efficient real-time operating system (RTOS), which provides a POSIX-style environment.

Figure 2.6: Pixhawk Flight Controller

Specifications are as follows:

- 68 MHz Cortex M4F CPU (256 KB RAM, 2 MB Flash)

  - Sensors: 3D Accelerometer / Gyroscope / Magnetometer / Barometer
  - Integrated backup, override and failsafe processor with mixing
  - MicroSD slot, 5 UARTs, CAN, I2C, SPI, ADC, etc

- **LIDAR**: The LIDAR-Lite v3 is a compact, high-performance optical distance measurement sensor from Garmin^{TM} as shown in Figure 5.8.

Figure 2.7: LIDAR-Lite v3

The specifications are as follows:

  - Range: 0-40m Laser Emitter
  - Accuracy: +/- 2.5cm at distances greater than 1m
  - Power: 4.755V DC; 6V Max
  - Current Consumption: 105mA idle; 130mA continuous
  - Rep Rate: 1500Hz
  - Laser Wave Length/Peak Power: 905nm/1.3 watts
  - Beam Divergence: 4m Radian × 2m Radian
  - Optical Aperture: 12.5mm
  - Interface: I2C or PWM

- **GPS**: GPS used is Ublox Neo-M8N GPS with Compass as shown in Figure 5.9.

Figure 2.8: Ublox Neo-M8N GPS

The specifications are as follows:

- 167 dBm navigation sensitivity
- Navigation update rate up to $10H_z$
- Cold starts: 26s
- $25 \times 25 \times 4$ mm ceramic patch antenna
- Rechargeable 3V lithium backup battery
- Low noise 3.3V regulator
- Diameter 60mm total size, 32 grams with case.

- **Motors and ESC Motor Controllers**: E800 Tuned Propulsion System is designed for multi-rotor copters. Shown in Figure 5.10

Figure 2.9: E800 Tuned Propulsion System by DJI

2.2.2 Camera Software and ROS nodes

ROS (Robot Operating System) provides libraries and tools to create robot applications. It provides hardware abstraction, device drivers, libraries, visualizers, message-passing, package

management, and more. ROS is licensed under an open source, BSD license (?, ?). The ROS-flea3 camera driver enables publishing of images on ROS topics which can in turn be viewed on rqt image view tool. The images can be viewed real time and are also stored in a rosbag. The screen capture of an instance of the camera view and ROS node running the rosbag to record to images is shown in figure

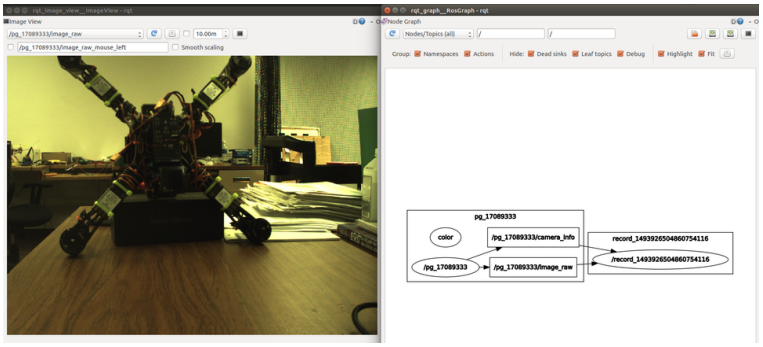

Figure 2.10: Camera view and the ROS-bag record running nodes on a Linux machine.

While the UAV is flying indoors or inside the bridge, it does not get a GPS signal for a better position estimate. Manual control is very difficult due to the smaller space and narrow pathways. In Chapter 3, we discuss the advantages of effectively learning obstacle avoidance or wall-following as a skill using the on-board sensor data. It is useful in these scenarios where the UAV needs to rely on its on-board sensors to perform a particular task simultaneously trying to avoid obstacles or follow a wall. Figure 5.12 indicates one such scenario where the UAV needs to take pictures inside the structures. The flight conducted at the VTTI smart road bridge was under manual control.

Figure 2.11: Indoor flight of the UAV visually inspecting the structure.

Pictures captured by the on-board camera are shown in Figure **??**.

Similar to the indoor bridge inspection, while flying close to the bridge surfaces, the UAV does not get reliable GPS signal or any other localization inputs. It is vital for the robot to

Figure 2.12: Pictures captured by the on-board camera at VTTI smart road bridge.

have learned the skill of flying close to the surfaces and following certain trajectories using on board laser sensor data. As iterated multiple times in this thesis, while learning in the real world, collecting negative samples (colliding with the wall/surface in this scenario) can lead to catastrophic results. It is important for the robot to learn a skill in a simulator environment before executing the required tasks in the real world. Figure 5.13 shows a picture of one of such flights for the outdoor visual inspection of the bridge. The flights were conducted at the VTTI smart road bridge.

We conducted another set of field experiments at the George Coleman Memorial Bridge, Yorktown, VA. it is a double swing bridge that spans the York River. It is a different type of bridge compared to the VTTI smart road bridge because of its movable span needed to allow ship access. The bridge spans over a river posing different challenges for UAV navigation compared to the VTTI smart road bridge.During the experiments at the George Coleman Memorial Bridge, the off the shelf controller was not able to hold position due to windy conditions.

The pictures from the flights at the George Coleman Memorial Bridge are shown in Figure **??**.

Pictures captured by the on-board camera are shown in Figure **??**.

A 3D reconstruction software Pix4D (?, ?) is used to create a 3D scan of the bridge from the images obtained during the flights shown in Figure **??**.

Figure 2.13: Outdoor flight of the UAV visually inspecting the structure at VTTI smart road bridge.

Figure 2.14: Outdoor flight of the UAV visually inspecting the structure at the Coleman Memorial Bridge.

bridge_img1.png

Figure 2.15: Images captured by the on-board camera at the Coleman Memorial Bridge.

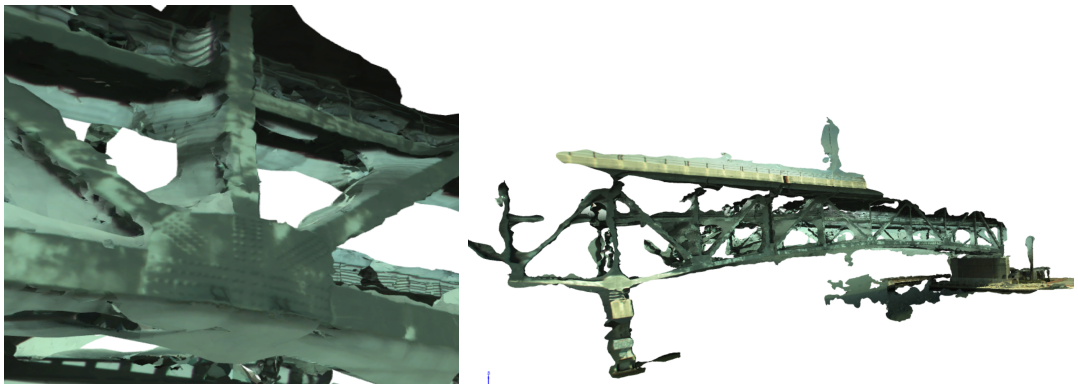

Figure 2.16: The 3D scan of the Coleman Memorial Bridge obtained from the collected images.

The unreliability of GPS and compass around these structures mean that relying on position for navigation is not recommended. Instead, this motivates the end-to-end perception based controller.

Chapter 3

Background

3.1 Sequential Decision Making

A delivery truck deciding which house to go first on a tour to deliver the packages, a robot exploring unknown environments, are all examples of sequential decision making. One of the main factors in sequential decision making is that the decisions made now can have both immediate and long term effects (27, 7). Sometimes it is effective to make a greedy choice but sometimes the decisions made depend critically on future situations. In the following sections, we review common sequential decision techniques.

3.1.1 Approaches to solve sequential decision making problems

Although in this thesis we are mainly interested in the algorithms which deal with *learning*, there exist other algorithms which are used to solve the problems related to sequential decision making. The following ways can be used in approaching sequential decision problems (50, 0). *Programming*: For each possible event/outcome, we can specify an action *a priori*. In most general, this is not possible due to the large state spaces of the problem or the intrinsic uncertainty of the environment or both. These solutions may work only for small problems with completely known static environments. *Search and Planning*: If we know the dynamics of a system, we can plan Search and Planning from a defined start state to a goal state. With uncertain actions, the standard algorithms do not work.

In contrast, *learning* offers many advantages to solve sequential decision making problems. There is no explicit need to perform the tedious task of programming all the possibilities in the design phase. Learning can effectively cope with uncertain environments, changing states and actions and reward oriented goal finding and lastly it can successfully solve the given problem for all the states and come up with a general policy.

3.1.2 Rewards, and how to assign them?

The important aspect of sequential decision making is the fact that, if the current action good or bad, cannot be decided right away. Sometimes the first action may have a large influence in reaching the goal even though the actions between the first one and the reward obtained at the end, may be bad. A formal model to represent such problems would be extremely useful in analyzing and solving sequential decision making problems. In Section 2.2 we would take a look at the most popular way to represent sequential decision making in an uncertain environment.

3.2 Markov Decision Processes

Markov Decision Processes are commonly used to model sequential decision making when the outcomes of the actions are uncertain.(38, 8). When an action is taken in a particular state, a reward is generated and a next state is attained through a particular transition probability.

Definition 1 *A Markov decision process is a tuple* (S, A, T, R) *in which* S *is a finite set of states,* A *a finite set of actions,* T *a transition function defined as* $T : S \times A \times S \to [0, 1]$ *and* R *a reward function defined as* $R : S \times A \times S \to \mathbb{R}$.

As seen in Definition 1, MDPs consist of states, actions, transitions between states and a reward function.

- States: The set of states S is defined as the finite set $\{s^1, ..., s^N\}$ where the size of the state space is N, *i.e.*, $|S| = N$. For example, for a robot moving in a $2D$ grid-world like environment, each position (x, y) may be represented as a unique state.
- Actions: The set of actions A is defined as the finite set $\{a^1, ..., a^M\}$ where the size of the action space is M, *i.e.*, $|A| = M$. Actions can be used to control the system state. The set of actions that can be applied in some particular state $s \in S$, is denoted $A(s)$, where $A(s) \subseteq A$. For examples, moving the robot forward, backward or sideways can be recognized as actions.
- The Transition Function: When an action $a \in A$ is applied in a state $s \in S$, then the agent makes transition to a state $s' \in S$. This transition is based on a probability distribution over all the states. The probability of ending in state s' when an action a is taken in s, is denoted by $T(s, a, s') \leq 1$.
- The Reward Function: The reward functions determines the reward obtained by the agent for being in a state or performing some action in a state, $R(s, a, s')$ defines the

reward obtained by the agent for performing action a in state s and it lands in state s'.

3.2.1 Policies

A policy for an MDP is a function which gives an action $a \in A$ that must be executed for each state $s \in S$. Formally, a deterministic policy π is a mapping from $\pi : S \rightarrow A$. Optimal policy π^* is computed and used by the agent to optimize its behavior in the environment modeled as an MDP.

3.2.2 Value function and Bellman equation

A *value function* represents an estimate of how good it is for the agent to be in a certain state (or how good it is to perform a certain action in that state). The notion of how good is expressed in terms of an optimality criterion, *i.e.*, in terms of the expected return.

The *value function* of a state s at time t under policy π denoted by $V^\pi(s)$ is the expected return when we start in the state s and follow the policy π after that. In an infinite horizon discounted model with discount factor γ, it is expressed as,

$$V^\pi(s) = \mathbb{E}_\pi \left\{ \sum_{k=0}^{\infty} \gamma^k r_{t+k} | s_t = s \right\} \tag{3.1}$$

A similar state-action value function $Q : S \times A \rightarrow R$ can be expressed as an expected return starting at state s, taking action a and following the policy π therefore,

$$Q^\pi(s, a) = \mathbb{E}_\pi \left\{ \sum_{k=0}^{\infty} \gamma^k r_{t+k} | s_t = s, a_t = a \right\} \tag{3.2}$$

For any policy π and state s, the Equation 2.1 can be recursively defined in terms of the *Bellman equation*(6,).

$$V^\pi(s_0) = \sum_{k=0}^{\infty} T(s_k, \pi(s_k), s_{k+1}) \Big(R(s_k, \pi(s_k), s_{k+1}) + \gamma V^\pi(s_{k+1}) \Big) \tag{3.3}$$

Equation 2.3 represents the expected value of a state s in terms of the immediate reward $R(s_k, a, s_{k+1})$ and the value of possible next states $V^\pi(s_{k+1})$ weighted by the transition probabilities $T(s_k, a, s_{k+1})$ with a discount factor of γ.

The goal is to find the best policy *i.e.*, the policy that maximizes the reward. An *optimal policy* denoted by π^* is such that $V^{\pi^*}(s) \geq V^{\pi}(s)$ for all $s \in S$ and all policies π. The optimal solution can be given by the *Bellman optimality equation* given in Equation 2.5

$$V^*(s) = \max_{a \in A} \sum_{s' \in S} T(s, a, s') \Big(R(s, a, s') + \gamma V^*(s') \Big) \tag{3.4}$$

Similarly, we can express the optimal state-action equation as,

$$Q^*(s, a) = \sum_{s'} T(s, a, s') \Big(R(s, a, s') + \gamma \max_{a'} Q^*(s', a') \Big) \tag{3.5}$$

In case of model-free approaches (Section 2.3.1) where T and R are unknown, the Q functions are learned instead of V functions. We can see the relation in Equation 2.6.

$$V^*(s) = \max_{a} Q^*(s, a) \tag{3.6}$$

We can find an optimal policy in case of model-free learning algorithms,

$$\pi^*(s) = arg \max_{a} Q^*(s, a) \tag{3.7}$$

The best action a in a particular state s is the one which has the highest expected reward based on the possible next state.

3.2.3 Solving MDPs

The two main dynamic programming methods to solve MDPs are policy iteration (19, 9) and value iteration (6,). In policy iteration the general policy iteration is separated into two steps whereas the latter represents a tight integration of policy evaluation and improvement. Policy iteration is a two step process. In policy iteration we start with an arbitrary initialized policy π_0. Then a sequence of iterations follows in which the current policy is evaluated after which it is improved. The first step, the policy evaluation step computes V^{π_k}. The second step, the policy improvement step, computes π_{k+1} from π_k using V^{π_k}. For each state, the optimal action is determined. If for all states s, $\pi_{k+1} = \pi_k$, the policy is stable and the policy iteration algorithm can stop.

However in value iteration, it is not necessary to wait for full convergence in the policy evaluation step. It is possible to stop evaluating earlier and improve the policy based on the evaluation obtained so far. The evaluation part can be stopped after the first step and it blends the policy improvement step into the iterations. The updates are done on the fly and the main goal is to directly estimate the value function.

3.3 Reinforcement Learning (RL)

Reference (8,) discusses learning the non-linear control for advanced stabilization of the UAVs whereas reference (29, 9) developed a high level control implementing learning strategies for high speed quadrotor multi flips. The system is able to do a series of flips for a quadrotor demonstrating online learning of acrobatics.

Some of the early examples of robot reinforcement learning are the OBELIX robot which learned to push boxes (30, 0) using value function-based approach. Carnegie Mellon's autonomous helicopter leveraged a model-based policy-search approach to learn a robust flight controller (5,). Kormushev and Calinon taught a robot the technique to flip pancakes (24, 4). The reinforcement learning algorithm explored in (42, 2) is Least Squares Policy Iteration (LSPI) to gain a fast learning process and a smooth landing trajectory. A recent paper (45, 5) applied reinforcement learning to a UAV to achieve stable hovering using the well known technique of Q-learning (Section 2.3.4). Unlike most of the studies, experiments using an actual quad rotor UAV were performed and the experimental results demonstrate that the UAV can acquire knowledge to achieve stable hovering over a marker placed on the ground.

Reinforcement Learning is a class of problems where the agent needs to learn the *behavior* with trial and error by interacting with a dynamic environment.

A simplified Reinforcement Learning Model can be represented as shown in Figure 2.1 The

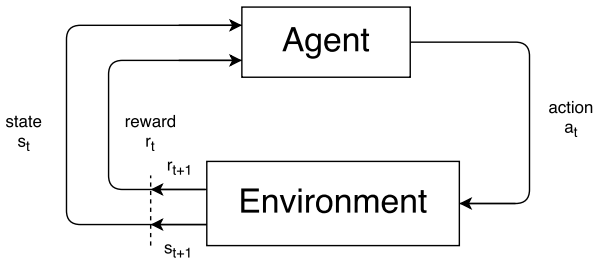

Figure 3.1: A Simplified Reinforcement Learning Model

environment is typically assumed to be stochastic *i.e.*, the same action in the same state at two different occasions may result in two different next states and/or two different rewards. The main difference between Reinforcement Learning and Supervised Learning is that, in RL, the agent needs to gather experience by interacting with the environment to find out the system states, transitions, actions and rewards whereas in Supervised Learning, some information about prior input/output pairs is used to approximate the mapping function.

3.3.1 Classification/Types

As we have seen previously, reinforcement learning agent needs to know the model of the environment; the transition function $T(s, a, s')$ and the reward function $R(s, a)$ in order to find an optimal policy. There are two broad approaches to solve this problem (20, 0).

- Model-free: Learn a controller without learning the model.
- Model-based: Learn the model of the environment in order to derive the controller.

A model is defined by the transition function $T(s, a, s')$ and the reward function $R(s, a)$.

Model-free

Model-free algorithms are the algorithms which do not have an explicit knowledge of the environment. The evaluation of how good the actions are is done by gathering samples. Model free algorithms tend to keep track of only the value functions whereas the model-based algorithms store the transition function $T(s, a, s')$ and the reward function $R(s, a)$.

Model-free algorithms need extensive experience to find an optimal policy. Examples of model-free algorithms are; Q-learning (49, 9) and SARSA (State Action Reward State Action)(41, 1).

Model-based

The online algorithms such as Q-learning guarantee convergence if the approximations are accurate. When the state-action space contains an infinite number of elements, it is impossible to loop over all the state-action pairs in finite time. Instead, a sample-based, approximate update has to be used that only considers a finite number of state-action samples. It is expensive to run these algorithms in the real world (18, 8). In model-based algorithms, an agent tries to learn the model of the environment while obtaining on-line experience and then this model can be used to facilitate learning.

$T(s, a, s')$ and $R(s, a)$ can be learned and be used during the further runs in order to improve the convergence. It is expected that, during the subsequent runs of the algorithm, the model should already be sufficiently learned to speed up convergence. Extensive amount of computation is required in model-based algorithms. A few examples of model-based reinforcement learning algorithms are ; $R\text{-}MAX$ (9,) and E^3 (21, 1).

The space complexity of model-free algorithms is considered to be asymptotically less than the space required to store an MDP (44, 4). Model-based algorithms are more data efficient. However, if the reward function is not known, it needs to be learned. Model-free algorithms

do not require explicit knowledge or learning of the reward function. A serious challenge for model-based approaches is overcoming inaccurate modeling. The policy found by these algorithm is only as good as the model of the environment. Both model-free and model-based approaches face challenges in handling high dimensional data (4,).

3.3.2 Online vs off-line learning

Consider a situation where the UAV needs to be trained to fly close to a surface without hitting obstacles. Learning the controller directly on the real task *online* is often difficult since learning a task needs a lot of data which is time consuming. More importantly, it is not very economic and *safe*, since there is a chance of the quad rotor colliding several times with the bridge causing damage. It is desirable to train the robot in a simulator which provides much faster and *safe* training situations where the agent can explore and can afford to make mistakes. *offline* learning uses a simulator of the environment as a cheap way to gather samples in a *fast* and a *safe* way. Often times one can use the simulators to obtain a reasonable policy for a given problem and then *fine tune* it in the real world. This thesis directly contributes to the development of such simulators training the UAVs to effectively navigate environments avoiding obstacles.

3.3.3 Exploration vs. Exploitation

An RL agent needs to explicitly explore the environment. One of the classic problems in the literature known as the *k-armed bandit problem* (7,) may best illustrate the concept of exploration vs. exploitation. The agent is in a room with a collection of k gambling machines. The agent is permitted a fixed number of pulls, z. Any arm may be pulled on each turn. The machines do not require a deposit to play; the only cost is in wasting a pull playing a suboptimal machine. When arm i is pulled, machine i pays 1 or 0, according to some underlying probability p_i, where the pays are independent events and the p_is are unknown. What should the agent's strategy be to maximize the payoffs?

The agent may believe that some arm may have a higher payoff probability. The question now is, whether to choose the same arm all the time or to explore the other arm that has less information but seems to be better? Depending on how long the game is going to last, if the game is going to last longer, then the agent should not converge to a sub-optimal arm too early and instead explore more. In short, exploitation means to use the knowledge that the agent has found for the current state s by doing one of the actions a that maximizes the value function of the state whereas exploration means, in order to build a better estimate of the optimal value function it should select a different action from the one that it currently thinks is best.

We will see one of the ways to trade of exploration-exploitation using ϵ-greedy strategy used

in Q-learning which is a form of model-free learning. The Section 2.3.1 describes the two fundamental types of Reinforcement Learning.

3.3.4 Q-Learning

In Q-learning is that we maintain a table $Q[s, a]$. In each state s we choose actions a that maximize the function $Q(s, a)$.

$$Q(s, a) = r(s, a) + \gamma \max_{a'}(Q(s', a')) \tag{3.8}$$

Input : S is a set of states
A is a set of action
γ is the discount factor
α is the learning rate or step size ($\alpha \in (0, 1)$)
Local data: Store the whole Q matrix $Q[S, A]$,
previous state s
previous action a,
next state s'
Initialize : Initialize $Q[S, A]$ arbitrarily/Zero
while *Termination condition not reached* **do**
  Choose an action a in the current state s based on the current Q-value estimates.
  Perform the action a in the state s and observe the current reward r and the next state s'.
  Update $Q(s, a) := Q(s, a) + \alpha[r(s, a) + \gamma \max_{a'} Q(s', a') - Q(s, a)]$:
end

Algorithm 1: Q-Learning Algorithm

The update equation given in Algorithm 1 updates the Q-value of the last state-action pair (s,a) with respect to the observed next state s' and the reward r with a learning rate parameter $\alpha \in (0, 1)$. Recalling Bellman update equation from Section 2.2.3, we can see that updated Q-value is the expected sum of the reward and discounted value of the next state. Unlike a general Bellman update equation, we are not marginalizing over all possible next states, since we have only observed one state here along with the reward for a particular state-action pair.

However, we can control the parameter α, which is the learning rate so as to allow the Q-value to change from its old estimate to a new estimate in the direction of the observed state and reward.

Example

Consider an agent that has to navigate through a grid given in the Figure 2.2. The walls in the grid block the agent's path. The actions taken by the agent are noisy *i.e.*, 80% of the time, the action North takes the agent North if there's no wall, 10% of the time action North takes the agent West, and 10% of the times to East. Each step taken by the agent has a small negative reward say, -0.25. A reward of $+1$ or -1 is given at the states shown in Figure 2.2. The goal of the agent is to maximize the sum of the rewards.

The agent has to store the Q values for each state-action pair ($Q(s, a)$). The space required to store the Q-table is $S \times A$. In this example, the number of states are 11 and number of possible actions are 4. A naive Q-Learning approach does not scale up to give faster solutions as the problem space grows.

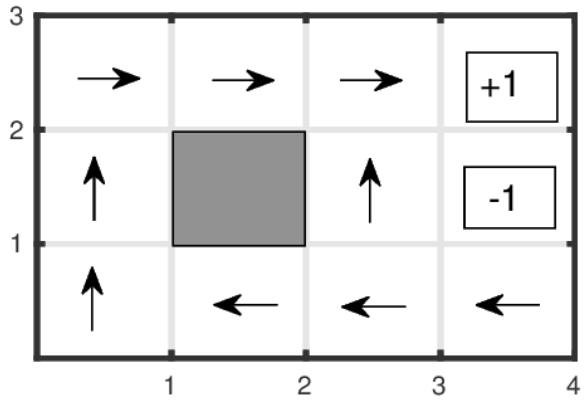

Figure 3.2: An example gridlworld with stochastic actions

Consider the following example. A robot (represented in green) with 6 laser beams is learning to navigate in an environment without colliding with obstacles of different sizes which are moving with different speeds. (The white obstacles move at slower speeds whereas the orange obstacle moves faster). The laser sensor can output distance values in the range 0 to 19. If we consider the state space to be the laser data $[l_1, l_2, l_3, l_4, l_5, l_6]$ and each of the 6 sensors can give 20 values, then we have a total of 2×10^6 possible states. This state space can be too large for a naive Q-Learning algorithm to achieve convergence. As we have seen in Section 2.3.1, model-free algorithms need extensive experience in order to compute optimal policies. To experience states of the order of 10^6 is a lengthy process. Instead, we will approximate the $Q[S, A]$ values using GP as function approximator.

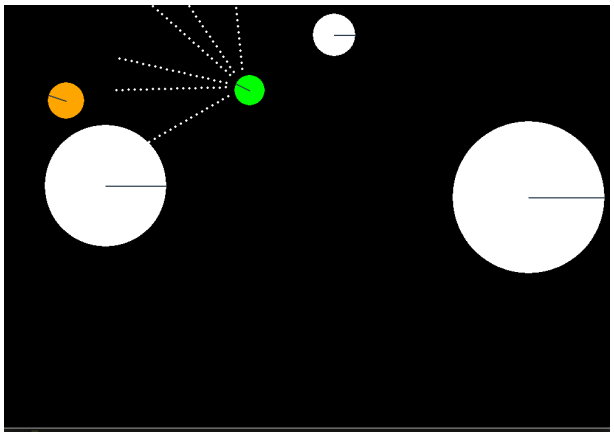

Figure 3.3: Navigation with perception in the loop

3.4 Introduction to Gaussian Processes (GP)

Consider a typical example of a prediction problem. Given some noisy observations at a certain values of the variable x, we wish to find the best estimate at a new value, x^*. We can assume the underlying function $f(x)$ to be some polynomial function and select an appropriate regression model to fit the given data. We have numerous possibilities of the function being a linear, quadratic or a cubic function.

Consider a least-square line fit $\hat{y} = p_0 + p_1 x$. We are specifying two parameters p_0 and p_1 for the Figure 2.4. A better fit would be to use a quadratic function say $\hat{y} = p_0 + p_1 x + p_2 x^2$. In this case, we need 3 parameters p_0, p_1 and p_2.

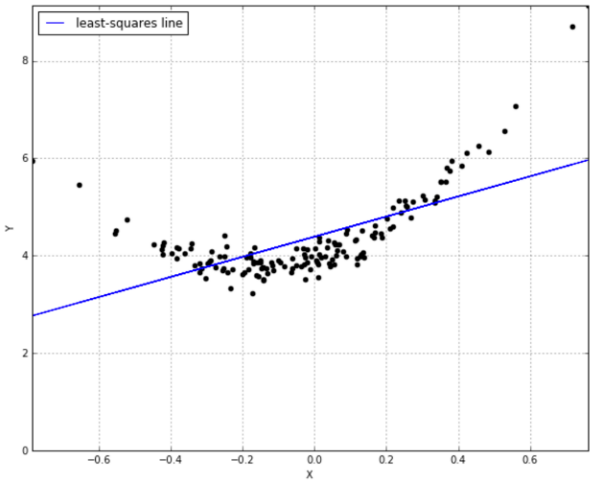

Figure 3.4: To find a function that is consistent over the observed data

Gaussian Process Regression provides a model-free approach in supervised learning in order to learn input-output mappings from empirical data.

A Gaussian Process(GP) is a generalization of the multivariate Gaussian distributions to infinite dimensions. A GP is considered to be a collection of random variables, any finite subset of which has a joint Gaussian distribution function. For example, a set of n data points $y = \{y_1, y_2, \ldots\ y_n\}$ can be considered as a single sample from an n-variate Gaussian distribution.

Kernel Functions

The relation between the observations is given by the *covariance function/ kernel function*, $k(x, x')$. A few basic kernels are defined below for input points x and x':

- Squared-Exponential (SE): This is a popular choice of a kernel function which is also known as the *Radial Basis Function* kernel (RBF). It has the following form.

$$k(x, x') = {\sigma_f}^2 \exp\left\{\frac{-(x - x')^2}{2l^2}\right\} \tag{3.9}$$

  where the maximum allowable covariance is defined as ${\sigma_f}^2$. $k(x, x')$ approaches this maximum when $f(x)$ is nearly perfectly correlated with $f(x')$.

- Periodic The periodic kernel allows one to model functions which repeat themselves exactly. It has the following form.

$$k_{Per}(x, x') = \sigma^2 \exp\left\{-\frac{2\sin^2(\pi|x - x'|/p)}{l^2}\right\} \tag{3.10}$$

- Linear Using a linear kernel in a GP, is equivalent to doing Bayesian linear regression. It has the following form.

$$k_{Lin}(x, x') = {\sigma_b}^2 + {\sigma_v}^2(x - c)(x' - c) \tag{3.11}$$

  - The offset c determines the x-coordinate of the point that all the lines in the posterior go though. The mean will be zero unless noise is added.
  - The constant variance ${\sigma_b}^2$ determines how far from 0 the height of the function will be at zero. It gives a prior to the value of the function instead of specifying the value of the function directly.

Each kernel has a number of parameters which are used to specify the precise shape of the covariance function. These are referred to as *hyper-parameters*, since they can be viewed as specifying a distribution over function parameters, instead of being parameters which

specify a function directly. An example would be the lengthscale parameter $l$of the RBF kernel, which specifies the width of the kernel and thereby the smoothness of the functions in the model.

Lengthscale l describes how smooth a function is. Small lengthscale value means that function values can change quickly, large values characterize functions that change only slowly. In general, we won't be able to extrapolate more than l units away from your data.

Signal variance σ^2 determines the average distance of your function away from its mean. It describes the variation of function values from their mean. (40, 0)

The SE and Periodic kernels are *stationary*. This implies that their value only depends on the difference $x - x'$. The probability of observing a particular dataset remains the same even if we move all the x values by some offset. In contrast, the linear kernel is *non-stationary*, This means that the corresponding GP model will produce different predictions if the data were moved while the kernel parameters were kept fixed.

3.4.1 Gaussian Process Regression

Given a joint probability distribution of the variables x_1 and x_2 as:

$$\begin{pmatrix} x_1 \\ x_2 \end{pmatrix} \sim \mathcal{N}\left(\begin{pmatrix} \mu_1 \\ \mu_2 \end{pmatrix}, \begin{pmatrix} \sigma_{11} & \sigma_{12} \\ \sigma_{21} & \sigma_{22} \end{pmatrix}\right) \tag{3.12}$$

It is possible to get the conditional probability of $x_1|x_2$ or vice-versa. In a GP, we can derive the posterior from the prior and the observations. The posterior is the joint probability of the values of the function of which some are observed (denoted by f) and some are not (denoted by f^*).

$$\begin{pmatrix} f \\ {f^*}_2 \end{pmatrix} \sim \mathcal{N}\left(\begin{pmatrix} \mu \\ \mu_* \end{pmatrix}, \begin{pmatrix} K & K_* \\ {K_*}^T & K_{**} \end{pmatrix}\right) \tag{3.13}$$

Here, K is the matrix we get by applying the kernel function to the observed values, *i.e.*the similarity between each observed x .K_* represents the similarity of the training values to the test values whose output values are to be estimated. K_{**} gives the similarity of the test values with each other. We are ultimately trying to determine $p(f_*|x_*, x, f)$ where f and f_* are jointly distributed as shown in equation 2.13. We ultimately are able to define the distribution $f_* \sim \mathcal{N}(\mu_*, \Sigma_*)$, where μ_* is the mean and Σ_* is the covariance matrix.

In model-based learning as stated in (40, 0), GPs can be used to model system dynamics. Assuming a set of N-dimensional observations of the form (s, a, s'), we can use separate Gaussian Process model for predicting each coordinate of the system dynamics. For example, the inputs can be the state-action pair (s, a) and the output is a multivariate Gaussian

distribution over the next state. In model-free learning, GPs can be used to model value functions as a function of states. We typically specify a finite number of data points $S = s_1, s_2, ..s_m$ and use GP to predict value of Q-function over the entire space.

The Gaussian processes offer nice properties such as uncertainty estimates over the function values, robustness to over-fitting, and principled ways for hyper-parameter tuning. In general, these useful properties of GPs are exploited in order to make them popular in terms of their use in machine learning.

3.5 Deep Reinforcement Learning

The conventional reinforcement learning focuses on linear function approximations and tabular representations (17, 7). To generalize in large and continuous state and action spaces, the linear approximations and tabular functions are not enough(34, 4). Performance of most of the successful RL applications operating in high dimensional sensor inputs like vision and speech rely on the quality of features along with the function approximations or policy representation. However in this study we explore the use of Gaussian Processes in reinforcement learning algorithms for UAV navigation.

Basic steps of applying RL to deep neural networks are the use of a deep network to represent value function or policy or model. The end-to-end optimization of this value function or policy or model and the use of Stochastic Gradient Decent to update the weights (31, 1). A naive representation of a Deep-Q network is shown in Figure 2.5.

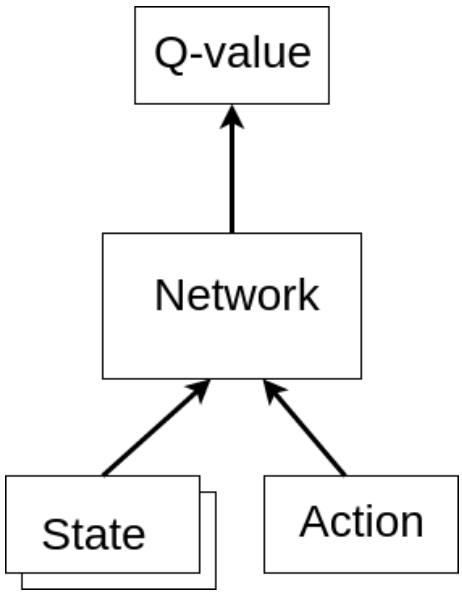

Figure 3.5: A naive representation of deep Q-network

Reference (25, 5) states that, with sufficient data fed into a deep neural network, it is often possible to learn better representations compared to handcrafted features. Reference (32, 2) describes a Deep-RL system which combines Deep Neural Networks with Reinforcement Learning at scale for the first time. This work represents the first demonstration of a general-purpose agent that is able to continually adapt its behavior without any human intervention. The algorithm given in (31, 1) is advantageous over an online Q-learning algorithm in the following ways. Each step of experience may be used in many weight updates which results in greater data efficiency. Due to strong correlation, learning from consecutive samples may be inefficient. Randomizing samples leads to decrease in covariance of the updates.

Chapter 4

The End-to-End GPQ Algorithm

In order for a robot to be able to navigate through an environment or perform a task of obstacle avoidance it needs to be equipped with sensors which are able to tell what surrounds it. The preliminary experiments reported in Chapter 5 motivate the need for robust navigation algorithms that do not rely on just positional sensors such as GPS and compass. Instead we present an algorithm that learns to navigate directly using onboard sensor input. We term this end-to-end learning.

The robot is equipped with a laser sensor (as shown in Figure 3.1) which provides the distance between the robot and its nearby obstacles. The task of the robot is to navigate through this environment without crashing into obstacles assuming the robot has no prior information about the environment and only has access to the real time laser data.

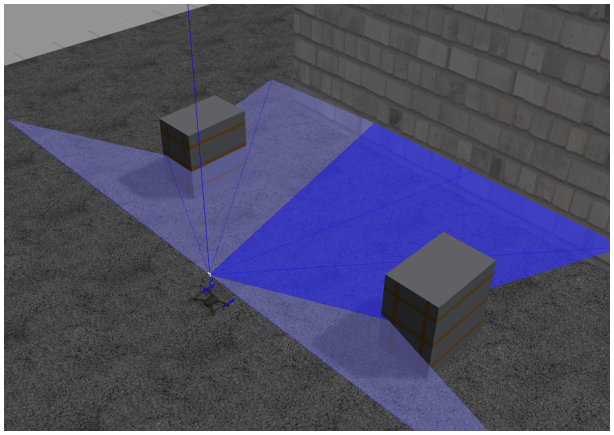

Figure 4.1: A UAV equipped with a laser sensor.

4.1 Laser data and Q-Learning

In order to learn the skill of obstacle avoidance, we decided to learn the mapping from sensor values to action. A naive Q-Learning algorithm was implemented (refer to algorithm 1) on the simulators described in Section 3.2. Building on the GPQ algorithm described in (10, 0), we present its novel application to UAV navigation using laser data. A Gaussian Process model of the value function (Q) is presented in (10, 0) in both batch and online settings. Our goal is to find out a function that approximates the Q values to fit the observed data. Given a set of observed state-action pairs (s, a) and the reward r, we calculate the Q values for the observed state-action pairs (s, a). Using Gaussian Process Regression (Section 2.4.1), we predict the Q values over the entire state space S (refer Algorithm 2).

The batch off-line algorithm may be considered in two phases.

- Training phase: Refer to the lines 1 to 9 in algorithm 2. Take a random action a in state s. Let the observed state and the reward be s' and r respectively. The new data (s, a, r, s') is added to the training set T. This loop is executed for a predefined number of iterations N.
- Batch GP-Q: From the training set T obtained in the training phase, the input to the GP extracted as dX, is the set of all state-action pairs (s, a). The target value is the sum of current reward r and the maximum value predicted by the GP for the next state s' over all actions $a \in A$ (returned by the function findMax(GP, s') line 20). The GP is updated with the input dX and the target vector tX (refer to line 18) and the loop is continued till the termination condition is not reached. (10, 0) show that the algorithm converges.

After we obtain the GP, an action $a^* = \mathit{findMax}(\texttt{GP}, s')$ is selected. The action is applied for a Δt time and the reward r is observed.

The online implementation of the algorithm is described below (Refer Algorithm 3).
First consider the naive implementation of the batch GPQ algorithm described in Algorithm 2. At each timestep t, the greedy action $a^* = \mathit{findMax}(\texttt{GP}, s')$ is selected with probability $1-\epsilon$ and with probability ϵ a random action is chosen. After each (s, a, r, s') experience, GP is updated by adding the new record. As the size of the record increases, the time required for GP computation grows in a cubic fashion. We modify the naive implementation such that a new experience will only be added to the GP if the reward obtained in that epoch (An *epoch* is defined as a fixed number of actions taken by the agent.) is less than a certain percentage of the sum of the reward obtained over time. This prevents the input to the GP from becoming too large over time.

```
1  trainingPhase()
       Input      : S is a set of states
                    A is a set of action
       Local data: store the training data T := {s, a, r, s'},
                    previous state s
                    previous action a
                    ,current reward r
                    next state s'
       Initialize : T ← empty
2      for i ∈ (1, N) do
3          s ← current state
4          a ← random action
5          Apply a for a Δt time
6          s' ← observed state
7          r ← observed reward
8          T ← T ∪ {(s, a, r, s')}
9      end
10 findMax(GP, s')
       Initialize : max ← 0
11     for a ∈ A do
12         temp ← gpPredict (s',a)
13         if temp > max then
14             max ← temp
15     end
16     return max
17 batchGPQ()
       Input      : T := (s, a, r, s') is the training set recorded during the training phase
       Initialize : Gaussian Process GP with RBF kernel of appropriate length scale
18     dX ← input to the GP
19     tX ← output of the GP.
20     for i ∈ (1, N) do
21         dX ← dX ∪ (s_i, a_i)
22         tX ← r_i + findMax(GP, s')
23     end
24     updateGP (dX, tX) return GP
25 main()
26     while do
27         termination condition not reached
28         GP = batchGPQ()
29         Choose action a* = findMax(GP, s')
30         Apply a* for a Δt time
31         observe reward r
32     end
```

Algorithm 2: Batch GPQ Algorithm

```
findMax(GP, s′)
    Initialize : max ← 0
    for a ∈ A do
        temp ← gpPredict (s′,a)
        if temp > max then
            max ← temp
    end
    return max
batchGPQ(GP, T)
    Input      : T := (s, a, r, s′) is the new experience obtained during runtime
    dX ← input to the GP
    tX ← output of the GP.
    for i ∈ (1, N) do
        dX ← dX ∪ (s_i, a_i)
        tX ← r_i + findMax(GP, s′)
    end
    updateGP (dX, tX) return GP
main()
    Initialize : T ← empty
    Initialize : Gaussian Process GP with RBF kernel of appropriate length scale
    while do
        termination condition not reached
        GP = batchGPQ(GP, T)
        s ← current state
        Choose greedy action a = findMax(GP, s′) with probability 1 − ϵ
        A random action is chosen with a probability ϵ
        Apply a for a Δt time
        s′ ← observed state
        r ← observed reward
        T ← T ∪ {(s, a, r, s′)}
        if r < .75 × sum of rewards over time then
            Update the GP using GP = batchGPQ(GP, T)
        end
    end
```

Algorithm 3: ϵ greedy online GPQ Algorithm

4.2 The Simulator setup

Two simulators were implemented in order to present the idea of perception and subsequently implementing the idea of reinforcement learning in order to learn a *skill*.

- **Simulator 1**: A python based obstacle avoidance simulator: As shown in Figure 3.2, the robot is trying to navigate without colliding with obstacles in a dynamic environment setting. The white obstacles move slower compared to the orange obstacle. The robot is equipped with a laser sensor which uses 6 beams in order to find out the distances from the obstacles at different angles. The robot has a constant speed and can perform 3 actions; turn left, turn right or stay in the same direction.

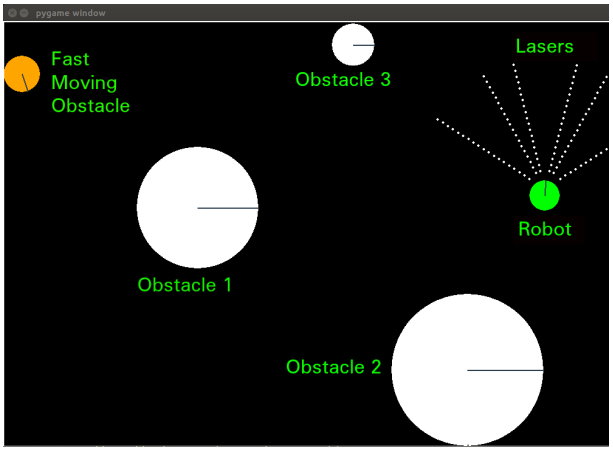

Figure 4.2: A python based simulator for obstacle avoidance.

- **Simulator 2**: A second simulator is implemented in the Gazebo robot simulator (23, 3). A UAV equipped with a Hokuyo Laser is implemented in the simulator as shown in Figure 3.3. This may be considered as a 3D extension of the simulator shown in Figure 3.2. With infinite state-action space and ability to add robot dynamics, this simulator is a higher fidelity simulator compared to the python-pygame based 2D simulator.

In both of the above simulators the main principle of *perception in the loop* is used in order to use the laser data to find out the current position of the obstacle with respect to the robot and take an optimal action in order to avoid the obstacle. In order to learn *obstacle avoidance* as a *skill* the algorithm must be agnostic to the shape or size of the obstacle and it should work in case of moving obstacles as well.

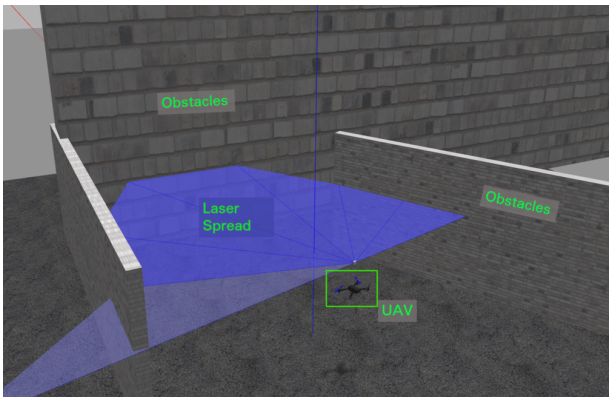

Figure 4.3: A UAV equipped with laser sensor in Gazebo Robot Simulator.

4.3 Simulations and Results

The performance of a batch-GPQ algorithm is compared with a naive Q-learning algorithm on the simulators shown in Figure 3.4. Similar to the Figure 3.2, we use three beams on the robot to gather the distance data. The goal of the robot is to navigate in the environment without colliding into the obstacles. A reward of -5 is given on collision and a positive reward which is a function of the sum of the laser values is awarded on being able to avoid colliding into obstacles.

4.3.1 Simulation Results

We carry out two types of experiments. In the first set of experiments, we train and test the performance of the agent in the same simulator. In the second type of experiments, we train the robot in simulator 1 shown in Figure 3.4 and test the performance in the Gazebo Robot simulator which is shown in Figure 3.6.

In order to compare the performance of the algorithms, we use *reward* as a metric of comparison. An *epoch* is defined as a set of fixed number of actions. The experiments are run in an online setting described in Algorithm 3. ϵ value is set to 0.1 for all the experiments. Reward r is collected over a set of 200 actions defined as one epoch. The plot shown in Figure 3.5, shows the reward obtained over 1000 epochs. The performance of the algorithm is compared with a naive Q learning algorithm run on the same set of environments with identical ϵ and epoch size.

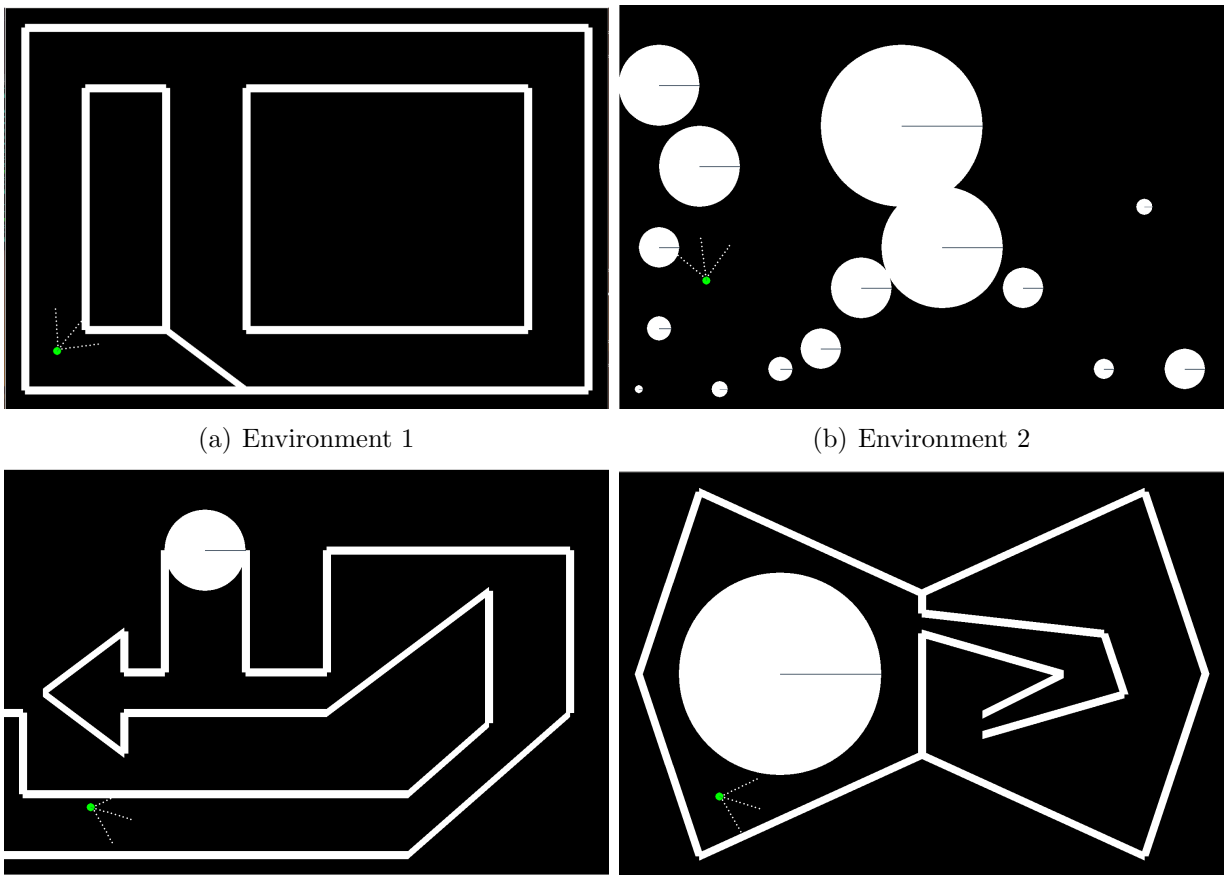

(a) Environment 1

(b) Environment 2

(c) Environment 3

(d) Environment 4

Figure 4.4: Simulator Environments.

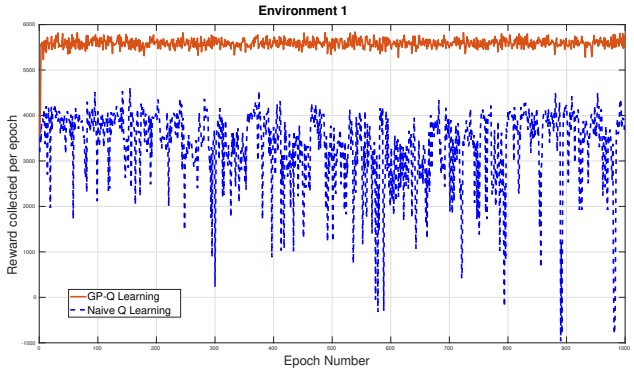

(a) Reward collected in Environment 1

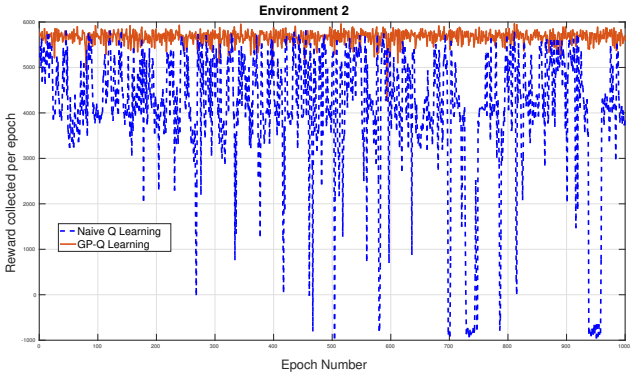

(b) Reward collected in Environment 2

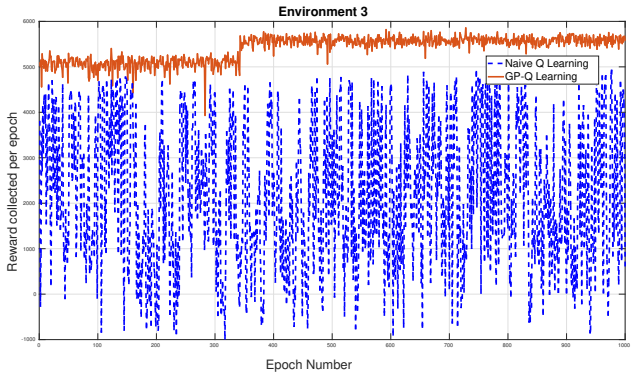

(c) Reward collected in Environment 3

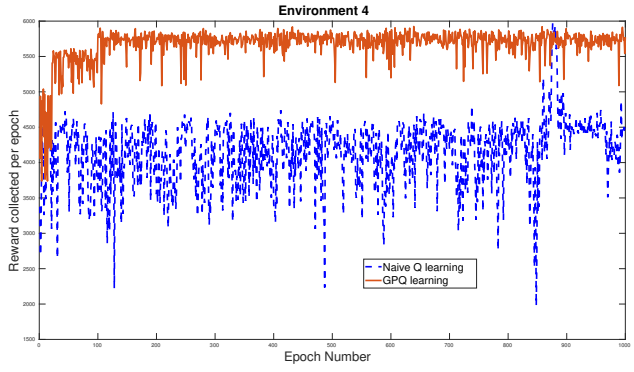

(d) Reward collected in Environment 4

The second set of experiments is performed in the Gazebo Robot Simulator. The GP learned in the basic kinematic simulators shown in Figure 3.4 is used directly to find the optimal policy to navigate the Gazebo Robot Simulator environments. An epoch is defined to be a set of 20 actions. Reward is collected over 200 such epochs and is plotted in Figure 3.6.

A naive Q learning algorithm is run in the same simulator in order to compare the performance of the two algorithms. It is evident from the plots that the GPQ algorithm where the agent is tested in a different simulator after learning the GP in the simulator shown in Figure 3.4 performs better than the naive Q learning algorithm.

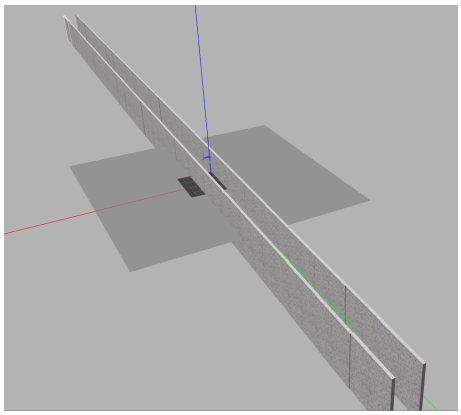

(a) Gazebo environment 1

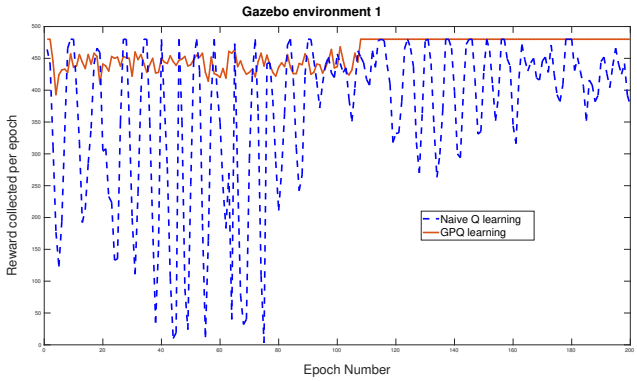

(b) Reward collected in Gazebo environment 1

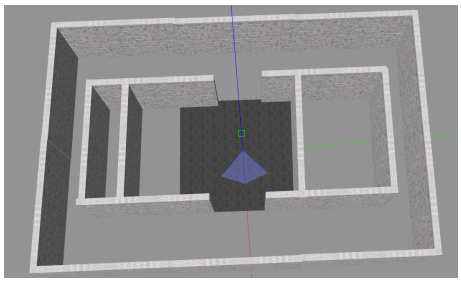

(c) Gazebo environment 2

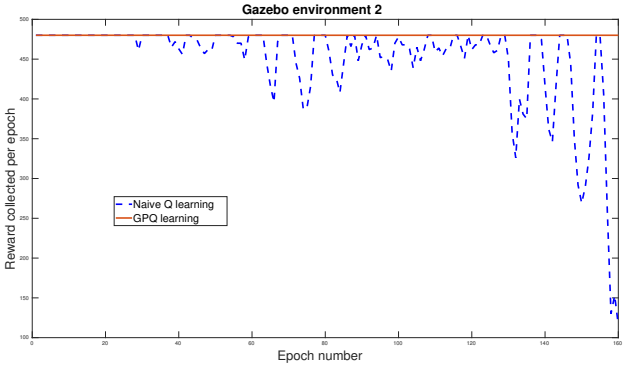

(d) Reward collected in Gazebo environment 2

Figure 4.6: Gazebo Robot Simulator environments and the reward collected over time. One *epoch* is a set of 20 actions.

The UAV model equipped with laser range sensors in the Gazebo Robot Simulator could effectively avoid obstacles in completely different environments by using the optimal policy learned in the lower fidelity simulator *i.e.*. the python based basic kinematic simulator. It is empirically shown that the GPQ algorithm performs better than the naive Q learning algorithm and it can be extended to a multi-fidelity simulator chain in order to further reduce

the number of samples required in the real world. The next chapter presents Multi-Fidelity Reinforcement Learning technique combined with GPs.

Chapter 5

The GP-MFRL Algorithm

In this chapter,the use of GP regression to learn the transition function is described and the details about the GP-MFRL algorithm are presented. This chapter emphasizes mainly on model-based approaches but can also be applied to model-free scenarios explained in the previous chapter.

5.1 Multi-Fidelity Reinforcement Learning

We build our work upon a recently proposed Multi-Fidelity Reinforcement Learning (MFRL) algorithm by Cutler et al. (12, 2). MFRL leverages multiple simulators to minimize the number of real world (*i.e.*, highest fidelity simulator) samples. The simulators denoted by $\Sigma_0, \ldots, \Sigma_D$, have increasing levels of fidelity with respect to the real environment. For example, Σ_0 can be a simple simulator that models only the robot kinematics, Σ_1 can model the dynamics as well as kinematics, Σ_2 can additionally model the wind disturbances, and the highest fidelity simulator can be the real world (Figure 4.1).

MFRL differs from transfer learning (47, 7) where transfer of parameters is allowed only in one direction. The MFRL algorithm starts in Σ_0. Once it learns an optimal policy in Σ_0, it switches to a higher fidelity simulator. If it observes that the policy learned in lower fidelity simulator is no longer optimal in the higher fidelity simulator, it either switches back to a lower fidelity simulator or stays at the same level. It was shown that the resulting algorithm has polynomial sample complexity and minimizes the number of samples required from the highest fidelity simulator.

The original MFRL algorithm uses Knows-What-It-Knows (KWIK) framework (26, 6) to learn the transition and reward functions in each level. The algorithm essentially maintains a mapping from a state-action pair to the learned reward and the next state. The reward and the transition for each state-action pair is learned independently of others. While this

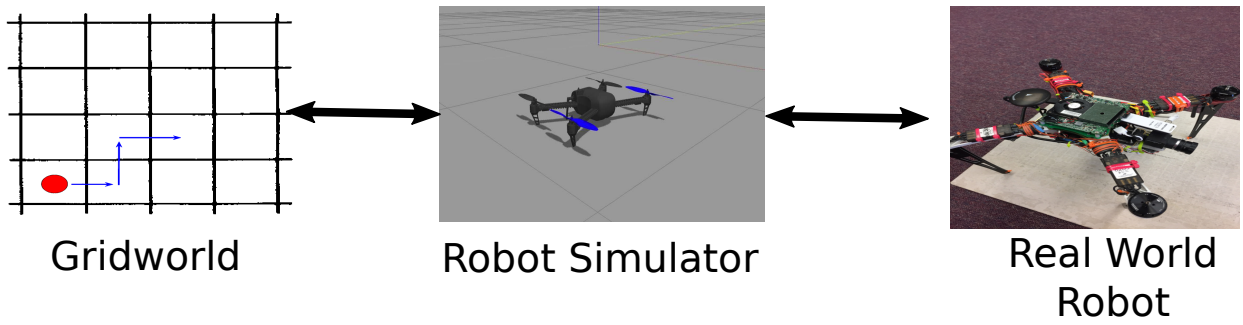

Figure 5.1: MFRL framework: First simulator captures only gridworld movements of a point robot while second simulator has more fidelity using a physics simulator. Control can switch back and forth between simulators and real environment which is essentially the third simulator in the multi-fidelity simulator chain.

is reasonable for general agents, in case of planning for robots we can exploit the spatial correlation between neighboring state-action pairs to speed up the learning. Our main contribution in this paper is to show how to use Gaussian Process (GP) regression to learn the transition function in an MFRL framework using fewer samples.

GPs are commonly used to learn transition models for agents moving in the real world (13, 3) and have been used in RL to learn the transition function (40, 0), the reward function (15, 5) and the value function (16, 6). GPs can predict the learned function for any query state-action pair, and not just for the discretized set of state-action pairs used when planning. In MFRL, the state space of Σ_i is a subset of the state space of Σ_j for all $j > i$. Therefore, when the MFRL algorithm switches from Σ_i to Σ_{i+1} it already has an estimate for the transition function for states in $\Sigma_{i+1} \setminus \Sigma_i$. Thus, GPs are particularly suited for MFRL which we verify through our simulation results.

5.2 Learning Transition Dynamics as a GP

A Markov Decision Processes (MDP) (38, 8) is defined by a tuple: $\langle S, A, \mathcal{R}^a_{ss'}, \mathcal{P}^a_{ss'}, \gamma \rangle$. S and A are the set of states and actions respectively. $\mathcal{R}^a_{ss'}$, referred to as reward dynamics, defines the reward received by the agent in making a transition from state s to s' while taking action a and $\mathcal{P}^a_{ss'}$ is the probability of making this transition (also referred to as transition dynamics).

Generally the agent does not know the reward it will receive after making a transition nor does it know the next state it will land in. The agent learns these parameters through interactions with the environment which is subsequently used to plan an optimal policy to earn the maximum expected reward, *i.e.*, $\pi^* : S \to A$.

RL algorithms are broadly classified into *model-free* learning and *model-based* learning as seen

in Section 2.3. Approaches that explicitly learn transition dynamics and/or reward dynamics of an environment are known as model-based learning (9, ; 21, 1). The learned transition and reward dynamics can then be used to find the optimal policy using, for example, policy iteration or value iteration (46, 6) which are often referred to as *planners*. In contrast, Strehl et al. (44, 4) presented a model-free algorithm wherein the agent directly learns the value function and obtains the optimal policy. In this paper, we focus on model-based approaches and use GP regression to learn the transition dynamics.

Rasmussen and Kuss (40, 0) showed how to use GPs for carrying out model-based RL. They assumed that the reward dynamics are known and the transition and value function was modeled as a GP. We use the same assumption for ease of exposition. However, assuming reward dynamics to be known is not a critical requirement. In fact, reward dynamics can also be easily be modeled as GPs.

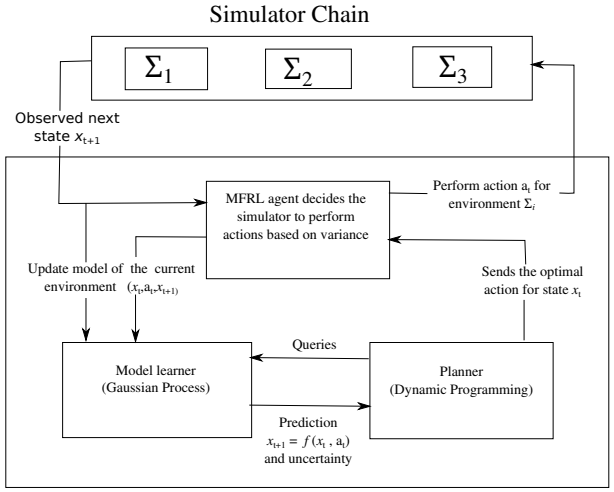

Figure 5.2: Overview of the GP-MFRL algorithm.

We observe a number of transitions: $\mathcal{D} = \{(\mathbf{x}_t, a_t, \mathbf{x}_{t+1})\}$. Let $\mathbf{x}_{t+1} = f(\mathbf{x}_t, a_t)$ be the (unknown) transition function that must be learned. Our goal is to learn an estimate $\tilde{f}(\mathbf{x}, a)$ of $f(\mathbf{x}, a)$ in as few samples in $\mathcal{D}$ as possible. We can then use this estimated $\tilde{f}$ for unvisited state-action pairs (in place of f) during value iteration to learn the optimal policy. f can also be a stochastic transition function, in which case, the GP estimate gives the mean and the variance of this noisy transition function. For a given state-action pair (s, a), the estimated transition function is defined by a normal distribution with mean and variance given by:

$$\mu_{(s,a)|\mathcal{D}} = \mathcal{K}_{(s,a)\mathcal{D}}\mathcal{K}_{\mathcal{D}\mathcal{D}}^{-1}\vec{\mathcal{X}}_{\mathcal{D}} \tag{5.1}$$

$$\sigma^2_{(s,a)|\mathcal{D}} = \mathcal{K}\{(s,a),(s,a)\} - \mathcal{K}_{(s,a)\mathcal{D}}\mathcal{K}_{\mathcal{D}\mathcal{D}}^{-1}\mathcal{K}_{(s,a)\mathcal{D}} \tag{5.2}$$

where $\mathcal{K}$ is the kernel function.

GP regression requires a kernel which encodes the correlation between the values of f at two points in the state-action space. Choosing a right kernel is the most crucial step in

implementing GP regression. We choose the Radial Basis Function (RBF) kernel for our implementation since it models the spatial correlation we expect to see in an aerial robot system well. However, any appropriate kernel can be used in our algorithm depending on the environment to be modeled.

RBF has infinite dimensional feature space and satisfies the Lipschitz smoothness assumption. It can be defined as follows: for two points $\mathbf{x}$ and $\mathbf{x'}$,

$$k(\mathbf{x}, \mathbf{x'}) = \exp\left(- \frac{||\mathbf{x} - \mathbf{x'}||^2}{2\sigma^2} \right) \tag{5.3}$$

where $||\mathbf{x} - \mathbf{x'}||^2$ is the squared Euclidean distance and σ is a hyperparameter for the kernel often known as *characteristic length-scale*. Here, $\mathbf{x}$ represents a point in the joint state-action space.

Instead of using GPs to predict the next state, we use it to predict the velocity with which the robot will move when a given action a_t is applied at a state s_t. Learning the velocity vector helps in transitioning between simulators as the size of the state space itself may be different. For example, one can construct a multi-fidelity simulator where Σ_0 is a $n \times n$ grid, Σ_1 is a denser $2n \times 2n$ grid, and so on. An action in Σ_0 moves the robot one unit whereas the same action in Σ_1 moves the robot only 0.5 units. By learning the velocity instead of the next state, we can scale the learned velocity function to easily compute the transition function in any Σ_i as:

$$\vec{\mathcal{V}}\ (s_t, a_t) = \frac{s_{t+1} - s_t}{\Delta_i} \tag{5.4}$$

where Δ_i is the time scaling of a simulator. If the state spaces of all simulators are the same, then one can use GPs to predict the next state instead of the velocity vector.

We train two GP regressions, $f_x, f_y : \mathbb{R}^4 \to \mathbb{R}$, assuming independence between the two output dimensions. Let (x_i, y_i) be the current state of the agent. Actions actions are represented using a tuple (a_x, a_y) where a_x and a_y can take the values between 0 or 1.

The GP prediction is used to determine the transitions, $(x_i, y_i, a_x) \to x_{i+1}$ and $(x_i, y_i, a_y) \to y_{i+1}$ where (x_{i+1}, y_{i+1}) is the predicted next state with variance σ_x and σ_y respectively. Value of hyperparameters is estimated by gradient descent by optimizing the maximum likelihood estimate of a training data set.

5.3 GP-MFRL Algorithm

Using multiple approximations of real world environments has previously been considered in the literature (3, ; 47, 7). Cutler et al. used model-based R-Max algorithm to reduce the number of samples using MFRL framework (12, 2). We use GP regression to further bring down the empirical sample complexity of MFRL framework.

Algorithm 4 gives the details of the proposed framework. As illustrated in Figure 4.2, there are two main components of GP-MFRL: (1) Model Learner; and (2) Planner. The model learner in our case is the GP-regression described in the previous subsection. We use value iteration (46, 6) as our planner to calculate the optimal policy on learned dynamics of environment.

An *epoch* measures the time span between two consecutive switches in the simulators. Before executing an action, the agent checks (Step 4) if it has a sufficiently accurate estimate of the transition dynamics for the current state-action pair in the lower fidelity simulator, Σ_{d-1}. If not, it switches to Σ_{d-1} and executes the action in the potentially less expensive environment. The function ρ^{-1} checks if the current state is also a valid state in the lower fidelity simulator.

We also keep track of the variance of the $\mathcal{L}$ most recently visited state-action pairs in the current epoch. If the running sum of the variances is below a threshold (Step 8), this suggest that the robot has found a good policy in the current simulator and it must advance to the next higher fidelity simulator.

Steps 12–16 in describe the main body where the agent computes the optimal action, executes it, and records the observed transition in $\mathcal{D}$. The GP model is updated after every n_U iterations (Step 17). In the update, we recompute the hyper-parameters until they converge.

A new policy is computed every time the robot reaches the goal state (Step 21). If the robot is in the highest fidelity simulator, we also check if the policy has converged by checking if the maximum change in the value function is less than a threshold (Step 22). If so, we terminate the learner.

5.4 Simulation Results

We demonstrate the GP-MFRL algorithm in a simulator chain consisting of a virtual grid-world environment and the Gazebo robot simulator (23, 3). The setup is shown in Figure 4.3. The simple grid-world agent operates in a 21×21 grid. The agent receives a reward of $+50$ at the goal location, and -1 for all other states. If the agent hits the obstacles, it gets the reward of -20. In each time step, an agent can move in one of the four directions viz. up, down, left and right. We add a Gaussian noise of σ to the actual transition to represent stochastic environments. The Gazebo simulation setup consists of a quadrotor with PX4 autopilot running in software–in–the–loop (SITL) mode. The PX4 SITL interfaces with the Robot Operating System (39, 9) via the `mavros` node.

The code is written in python and uses scikit-learn (37, 7) to implement GP-regression. The code is available online at `https://github.com/raaslab/gp_gazebo`.

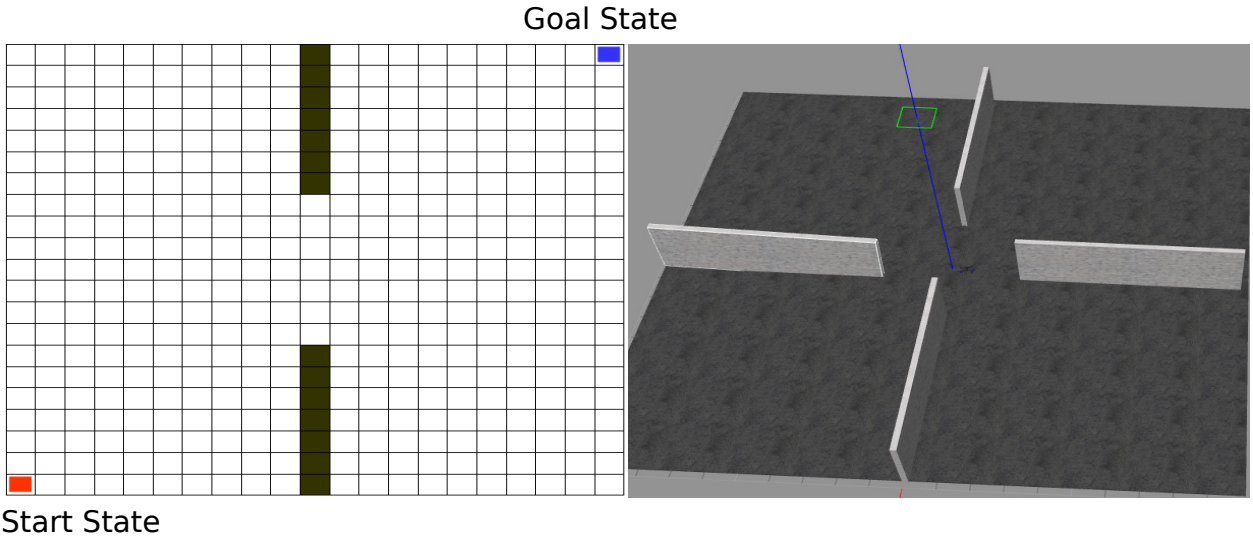

Figure 5.3: The environment setup for a multi-fidelity simulator chain. The simple gridworld environment has two wall obstacles whereas the gazebo environment has four wall obstacles as shown.

Figure 4.4 shows the switching between the simulators for one run of the GP-MFRL algorithm on the environment shown in Figure 4.3. It can be seen that the agent switches back and forth between the two simulators unlike unidirectional transfer learning algorithms. In the rest of the simulations we study the effect of the parameters used in GP-MFRL and the fidelity of the simulators on the number of samples till convergence.

Input : A simulator chain,
Confidence parameter ψ for (s, a),
History Length $\mathcal{L}$,
Confidence Ψ,
State mapping ρ,
Reward dynamics $\mathcal{R}^a_{ss'}$
Update rate n_U
Initialize: Transition dynamics $\mathcal{P}^a_{ss'}$;
$d = 1$;
$\mathcal{V}^*_d(s) \leftarrow$ `Planner` $(\mathcal{P}^a_{ss'})$

```
Learner()
```
while true **do**
  $a^*_t \leftarrow \text{argmax}_a\ \mathcal{V}^*_d(s_t)$;
  if $\sigma(\rho^{-1}(s_t, a^*_t)) \geq \psi\ \bigwedge\ d > 1$ **then** `// Return to level` $d-1$
    $d \leftarrow d - 1$;
    `epochLength` $\leftarrow\ 0$
  end
  if $\sum_{i=t-\mathcal{L}}^{t-1} \sigma(s_i, a^*_i) \leq \Psi\ \bigwedge$ `epochLength` $\geq \mathcal{L}$ **then**
    $d \leftarrow d + 1$ (Move up the simulator) ;
    `epochLength` $\leftarrow\ 0$;
  end
  $a^*_t \leftarrow \text{argmax}_a\ \mathcal{V}^*_d(s_t)$;
  Execute a^*_t and store observed s_{t+1}, r_{t+1} ;
  `epochLength` ++ ;
  $\mathcal{D}_t = \mathcal{D}_t \cup (s_t,\ a^*_t,\ s_{t+1})$;
  $s_t \leftarrow s_{t+1}$;
  if `epochLength` is multiple of n_U **then**
    $\mathcal{P}^a_{ss'} \leftarrow$ `UpdateGP`$(\mathcal{D}_t)$;
  end
  if s_t is Goal state **then**
    $\mathcal{V}_f(s) \leftarrow$ `Planner`$(\mathcal{P}^a_{ss'})$;
    if $\max_s\ \mathcal{V}_f(s) - \mathcal{V}_0(s) \leq 10\ \% \bigwedge d == D$ **then**
      break the loop ;
    end
    $\mathcal{V}_0(s) \leftarrow \mathcal{V}_f$;
  end
  $t \leftarrow t + 1$;
end

```
Planner()
```
Initialize: $\mathcal{V}(s) = 0,\ \forall(s, a)$
$\Delta = \infty$
while $\Delta > 0.1$ **do**
  for *every s:* **do**
    $temp \leftarrow \mathcal{V}(s)$;
    $\mathcal{V}(s) \leftarrow \max_a \sum_a \sum_{s'} \mathcal{P}^a_{ss'}[\mathcal{R}^a_{ss'} + \gamma\mathcal{V}(s')]$;
    $\Delta \leftarrow \max(0,\ |temp - \mathcal{V}(s)Init|)$
  end
end
return $\mathcal{Q}(s, a)$

Algorithm 4: GP-MFRL Algorithm

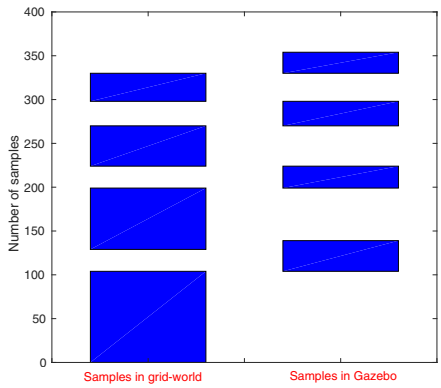

Figure 5.4: The figure represents the samples collected in each level of simulator for a 21×21 grid in a simple grid-world and Gazebo environments. Ψ and ψ were kept 0.4 and 0.1.

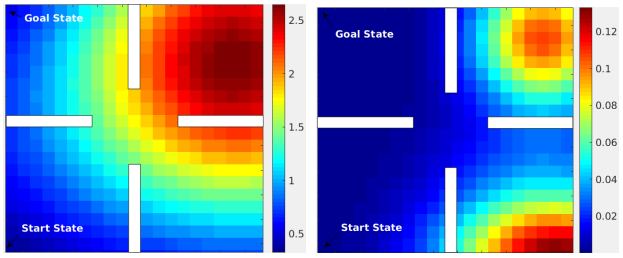

(a) After Initial Training (b) After Convergence

Figure 5.5: Variance plot for 21×21 multi-fidelity environment after transition dynamics initialization and after algorithm has converged.

5.4.1 Representative simulations

We first present three representative scenarios to observe the qualitative performance of the GP-MFRL algorithm. Specifically, we consider three instances and show how the variance evolves over time as more samples are collected. Recall that the main advantage with using GPs is that it allows for quick generalization of observed samples to unobserved state-action pairs.

To demonstrate how variance of the predicted transition dynamics varies from the beginning of experiment to convergence, we plot "heatmaps" of the variance. The GP prediction for a state-action pair also gives the variance, σ_x and σ_y, respectively for the predicted state. The heatmap shows $\sqrt{\sigma_x^2 + \sigma_y^2}$ for the optimal action at every state as returned by the Planner.

Figures 4.5 and 4.6 show the heatmaps at the start and convergence for the same environment but with different start and goal positions. As expected, the variance along the optimal (*i.e.*, likely) path is low whereas the variance for states unlike to be on the optimal path from start to goal remains high.

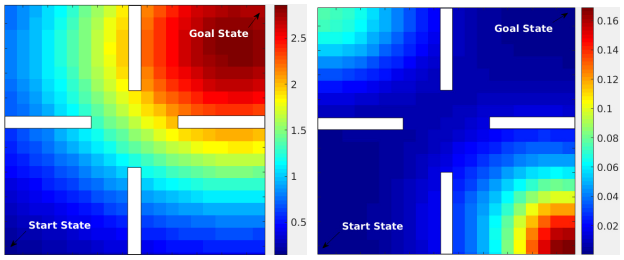

(a) After Initial Training (b) After Convergence

Figure 5.6: Variance plot for 21 × 21 multi-fidelity environment after transition dynamics initialization and after algorithm has converged

A more interesting case is presented in Figure 4.7. Even though there's a path available to reach the goal from the right of wall A, the agent explores that region less than the region near the walls B, C and D (indicated in dark blue showing less variance). This is due to the fact that, the transition dynamics learned in the lower fidelity simulator is used in the higher fidelity simulator leading to lesser exploration of the regions which are not along the optimal path.

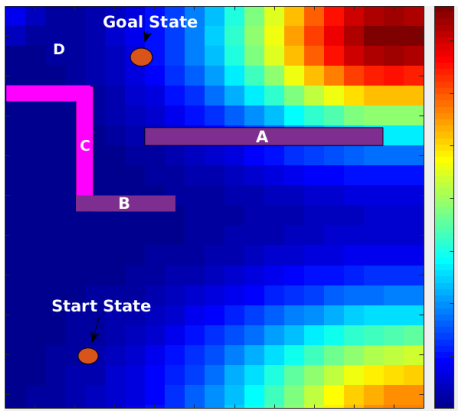

Figure 5.7: Variance plot for 21 × 21 multi-fidelity environment after the algorithm has converged. Walls A and B are only present in the grid-world simulator, whereas all four walls are present in the Gazebo simulator.

5.4.2 Effect of fidelity on the number of samples.

We first study the effect of varying fidelity on the total number of samples and the fraction of the samples collected in the higher fidelity simulator. Our hypothesis is that having learned the transition dynamics in the gridworld, the agent will need fewer samples in the higher fidelity Gazebo simulator to find the optimal policy. However, as the fidelity of the first

simulator decreases, we would need more samples in Gazebo.

In order to validate this hypothesis, we varied the noise parameter used to simulate the transitions in the gridworld. The transition model in Gazebo remains the same. The total number of samples collected increases as we increase the noise in gridworld (Figure 4.8). As we increase the noise in the first simulator, the agent learns less accurate transition dynamics leading to collection of more number of samples in the higher fidelity simulator. Not only does the agent need more samples, the ratio of the samples collected in the higher fidelity simulator to the total number of samples also increases (Figure 4.9).

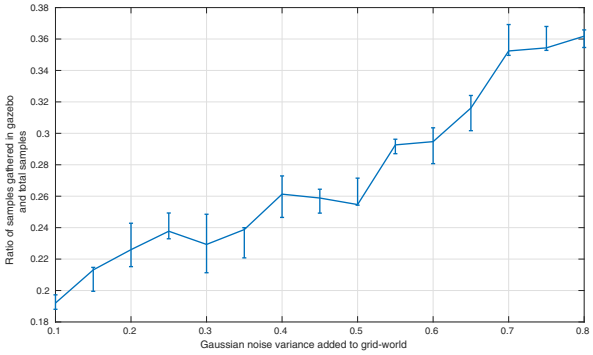

Figure 5.8: As we make first simulator more inaccurate by adding noise, the agent tends to gather more samples in second simulator.

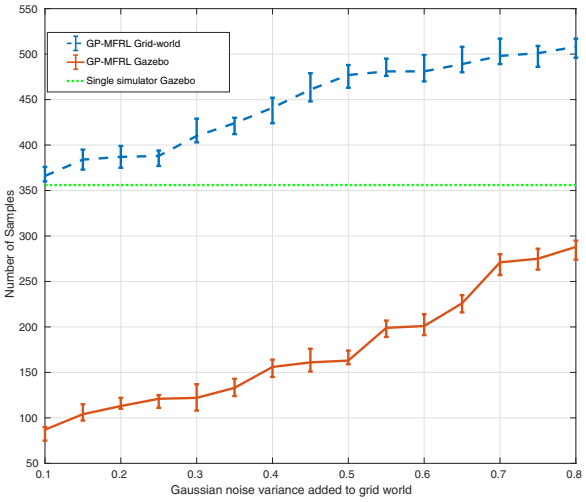

Figure 5.9: Ratio of samples gathered in the second simulator to the total samples gathered increases with inaccuracy in the first simulator. The reference line depicts the average number of samples gathered over 10 runs when only Gazebo simulator was present.

5.4.3 Effect of the confidence parameters.

The GP-MFRL algorithm uses two confidence parameters, ψ and Ψ, which are compared against the variance in the transition dynamics to switch to a lower and higher simulator, respectively. Figure 4.10 shows the effect of varying the two parameters on the ratio of number of samples gathered in the Gazebo simulator to the total number of samples. As expected, increasing ψ or decreasing Ψ leads to more samples being collected in the higher fidelity simulator.

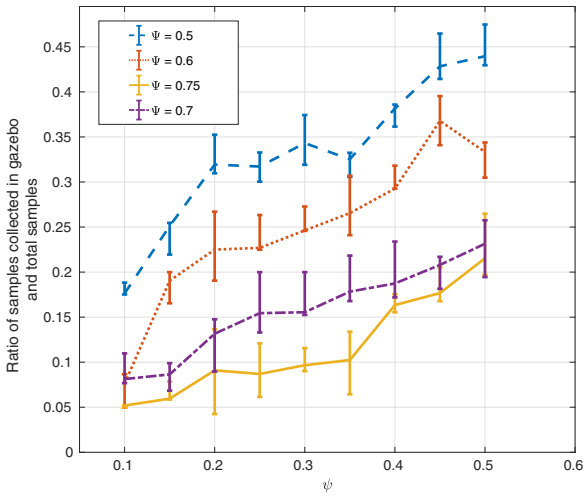

Figure 5.10: Ratio of samples gathered in second simulator vs. total samples gathered as we change the threshold or confidence parameters of the two simulators.

5.4.4 Comparison with R-max MFRL

Figure 4.11 shows the comparison between performance of GP-MFRL algorithm with the existing MFRL algorithm (12, 2), GP-MFRL algorithm only in the highest fidelity simulator and Rmax algorithm running only in the highest fidelity simulator. The experiments are performed in the environment same as the one used in Figure 4.7. As expected, the GP-MFRL algorithm performs better than the existing MFRL algorithm, (12, 2).

5.5 Conclusion

The GP-MFRL algorithm provides a general RL technique that is particularly suited for robotics. An extension to the existing work would be implementing the GP-MFRL algorithm on an actual quadrotor as the highest-fidelity simulator to demonstrate the utility of GP-

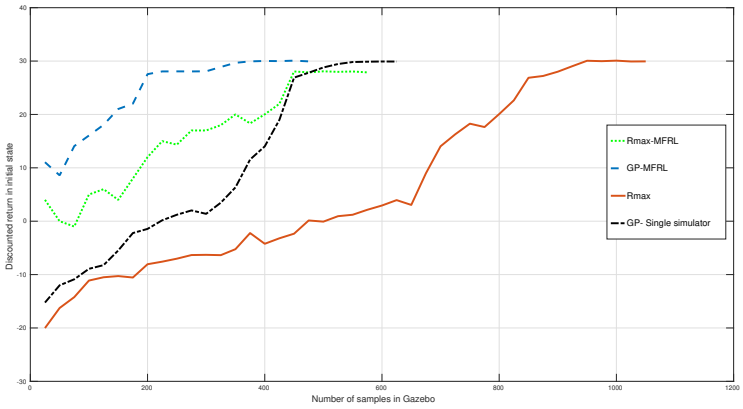

Figure 5.11: Discounted return in the start state Vs. the number of samples collected in the highest fidelity simulator.

MFRL. In this thesis, it is shown empirically that, GP-MFRL finds optimal policies using fewer samples than MFRL algorithm.

Chapter 6

Conclusion and Future Research

The GP-MFRL algorithm provides a general RL technique that is particularly suited for robotics. Our immediate work focuses on extending the End-to-End GPQ algorithm to a multi-fidelity simulator framework. Implementing the algorithm on an actual quadrotor as the highest fidelity simulator to demonstrate the utility of GP-MFRL is the immediate goal. We analyze empirically that GP-MFRL and GPQ find optimal policies in fewer samples than their naive counterparts. One of the main tasks is to find the theoretical bounds on the sample complexity of GP-MFRL.

In End-to-End GPQ algorithm, as the number of observations increase, the time taken to perform GP updates also increases with a cubic order. We can use adaptive sample selection techniques (35, 5) as well as numerical optimization techniques (16, 6) to speed up this process. Our ongoing work on sparse online Gaussian Processes (11, 1) should be able to overcome the limitations for larger data sets in order to perform online GP prediction of Q values instead of off-line batch predictions.

Theoretical and simulation results are useful in defining the performance limits and this level of abstraction is useful in providing insight to the research direction and making progress. However, it is important to bridge the gap between these results and practical limitations in order to deploy intelligent robots in realistic environments. The motivating example of bridge inspection is one such example of a real environment. Our goal is to be able to successfully perform autonomous navigation of UAVs in such environments.

Bibliography

DJI F-450 Frame. `http://www.dji.com/flame-wheel-arf/spec`. Accessed: 2016-05-25.

Flea3 2.0 MP Camera. `https://www.ptgrey.com/flea3-20-mp-color-usb3-vision-e2v-ev76c5706f-3`. Accessed: 2016-05-25.

Pieter Abbeel, Morgan Quigley, and Andrew Y Ng. Using inaccurate models in reinforcement learning. In *Proceedings of the 23rd international conference on Machine learning*, pages 1–8. ACM, 2006.

Christopher G Atkeson and Juan Carlos Santamaria. A comparison of direct and model-based reinforcement learning. In *Robotics and Automation, 1997. Proceedings., 1997 IEEE International Conference on*, volume 4, pages 3557–3564. IEEE, 1997.

J Andrew Bagnell and Jeff G Schneider. Autonomous helicopter control using reinforcement learning policy search methods. In *Robotics and Automation, 2001. Proceedings 2001 ICRA. IEEE International Conference on*, volume 2, pages 1615–1620. IEEE, 2001.

Richard Bellman. *Dynamic Programming*. Princeton University Press, Princeton, NJ, USA, 1 edition, 1957.

Donald A Berry and Bert Fristedt. *Bandit problems: sequential allocation of experiments (Monographs on statistics and applied probability)*. Springer, 1985.

Haitham Bou-Ammar, Holger Voos, and Wolfgang Ertel. Controller design for quadrotor uavs using reinforcement learning. In *Control Applications (CCA), 2010 IEEE International Conference on*, pages 2130–2135. IEEE, 2010.

Ronen I Brafman and Moshe Tennenholtz. R-max-a general polynomial time algorithm for near-optimal reinforcement learning. *Journal of Machine Learning Research*, 3(Oct):213–231, 2002.

Girish Chowdhary, Miao Liu, Robert Grande, Thomas Walsh, Jonathan How, and Lawrence Carin. Off-policy reinforcement learning with gaussian processes. *IEEE/CAA Journal of Automatica Sinica*, 1(3):227–238, 2014.

Lehel Csató and Manfred Opper. Sparse on-line gaussian processes. *Neural computation*, 14(3):641–668, 2002.

Mark Cutler, Thomas J Walsh, and Jonathan P How. Reinforcement learning with multi-fidelity simulators. In *2014 IEEE International Conference on Robotics and Automation (ICRA)*, pages 3888–3895. IEEE, 2014.

Philip Dames, Pratap Tokekar, and Vijay Kumar. Detecting, localizing, and tracking an unknown number of moving targets using a team of mobile robots. In *International*

Symposium on Robotics Research (ISRR). 2015.

Jnaneshwar Das, Gareth Cross, Chao Qu, Anurag Makineni, Pratap Tokekar, Yash Mulgaonkar, and Vijay Kumar. Devices, systems, and methods for automated monitoring enabling precision agriculture. In *Proceedings of IEEE Conference on Automation Science and Engineering*, pages 462–469. IEEE, 2015.

Marc Peter Deisenroth. *Efficient reinforcement learning using Gaussian processes*, volume 9. KIT Scientific Publishing, 2010.

Yaakov Engel, Shie Mannor, and Ron Meir. Reinforcement learning with gaussian processes. In *Proceedings of the 22nd international conference on Machine learning*, pages 201–208. ACM, 2005.

Atari Game. Deep reinforcement learning.

Todd Hester, Matej Vecerik, Olivier Pietquin, Marc Lanctot, Tom Schaul, Bilal Piot, Andrew Sendonaris, Gabriel Dulac-Arnold, Ian Osband, John Agapiou, et al. Learning from demonstrations for real world reinforcement learning. *arXiv preprint arXiv:1704.03732*, 2017.

Leslie Pack Kaelbling, Michael L Littman, and Anthony R Cassandra. Planning and acting in partially observable stochastic domains. *Artificial intelligence*, 101(1):99–134, 1998.

Leslie Pack Kaelbling, Michael L Littman, and Andrew W Moore. Reinforcement learning: A survey. *Journal of artificial intelligence research*, 4:237–285, 1996.

Michael Kearns and Satinder Singh. Near-optimal reinforcement learning in polynomial time. *Machine Learning*, 49(2-3):209–232, 2002.

Jens Kober and Jan Peters. Reinforcement learning in robotics: A survey. In *Reinforcement Learning*, pages 579–610. Springer, 2012.

Nathan Koenig and Andrew Howard. Design and use paradigms for gazebo, an open-source multi-robot simulator. In *Intelligent Robots and Systems, 2004.(IROS 2004). Proceedings. 2004 IEEE/RSJ International Conference on*, volume 3, pages 2149–2154. IEEE, 2004.

Petar Kormushev, Sylvain Calinon, and Darwin G Caldwell. Robot motor skill coordination with em-based reinforcement learning. In *Intelligent Robots and Systems (IROS), 2010 IEEE/RSJ International Conference on*, pages 3232–3237. IEEE, 2010.

Alex Krizhevsky, Ilya Sutskever, and Geoffrey E Hinton. Imagenet classification with deep convolutional neural networks. In *Advances in neural information processing systems*, pages 1097–1105, 2012.

Lihong Li, Michael L Littman, Thomas J Walsh, and Alexander L Strehl. Knows what it knows: a framework for self-aware learning. *Machine learning*, 82(3):399–443, 2011.

Michael Lederman Littman. *Algorithms for sequential decision making*. PhD thesis, Brown University, 1996.

Peter Liu, Albert Y Chen, Yin-Nan Huang, J Han, J Lai, S Kang, T Wu, M Wen, and M Tsai. A review of rotorcraft unmanned aerial vehicle (uav) developments and applications in civil engineering. *Smart Struct. Syst*, 13(6):1065–1094, 2014.

Sergei Lupashin, Angela Schöllig, Michael Sherback, and Raffaello D'Andrea. A simple learning strategy for high-speed quadrocopter multi-flips. In *Robotics and Automation*

(ICRA), 2010 IEEE International Conference on, pages 1642–1648. IEEE, 2010.

Sridhar Mahadevan and Jonathan Connell. Automatic programming of behavior-based robots using reinforcement learning. *Artificial intelligence*, 55(2-3):311–365, 1992.

Volodymyr Mnih, Koray Kavukcuoglu, David Silver, Alex Graves, Ioannis Antonoglou, Daan Wierstra, and Martin Riedmiller. Playing atari with deep reinforcement learning. *arXiv preprint arXiv:1312.5602*, 2013.

Volodymyr Mnih, Koray Kavukcuoglu, David Silver, Andrei A Rusu, Joel Veness, Marc G Bellemare, Alex Graves, Martin Riedmiller, Andreas K Fidjeland, Georg Ostrovski, et al. Human-level control through deep reinforcement learning. *Nature*, 518(7540):529–533, 2015.

G Morgenthal and N Hallermann. Quality assessment of unmanned aerial vehicle (uav) based visual inspection of structures. *Advances in Structural Engineering*, 17(3):289–302, 2014.

Jeremy Morton. Deep reinforcement learning. 2016.

Michael Osborne. *Bayesian Gaussian processes for sequential prediction, optimisation and quadrature*.

Tolga Ozaslan, Shaojie Shen, Yash Mulgaonkar, Nathan Michael, and Vijay Kumar. Inspection of penstocks and featureless tunnel-like environments using micro uavs. In *International Conference on Field and Service Robotics*, 2013.

F. Pedregosa, G. Varoquaux, A. Gramfort, V. Michel, B. Thirion, O. Grisel, M. Blondel, P. Prettenhofer, R. Weiss, V. Dubourg, J. Vanderplas, A. Passos, D. Cournapeau, M. Brucher, M. Perrot, and E. Duchesnay. Scikit-learn: Machine learning in Python. *Journal of Machine Learning Research*, 12:2825–2830, 2011.

Martin L Puterman. *Markov decision processes: discrete stochastic dynamic programming*. John Wiley & Sons, 2014.

M. Quigley, B. Gerkey, K. Conley, J. Faust, T. Foote, J. Leibs, E. Berger, R. Wheeler, and A. Ng. ROS: an open-source Robot Operating System. In *ICRA Workshop on Open Source Software*, 2009.

Carl Edward Rasmussen and Malte Kuss. Gaussian processes in reinforcement learning. 2003.

Gavin A Rummery and Mahesan Niranjan. *On-line Q-learning using connectionist systems*. University of Cambridge, Department of Engineering, 1994.

Marwan Shaker, Mark N. R. Smith, Shigang Yue, and Tom Duckett. Vision-based landing of a simulated unmanned aerial vehicle with fast reinforcement learning. In *Proceedings of the 2010 International Conference on Emerging Security Technologies*, EST '10, pages 183–188, Washington, DC, USA, 2010. IEEE Computer Society.

William D Smart and L Pack Kaelbling. Effective reinforcement learning for mobile robots. In *Robotics and Automation, 2002. Proceedings. ICRA'02. IEEE International Conference on*, volume 4, pages 3404–3410. IEEE, 2002.

Alexander L Strehl, Lihong Li, Eric Wiewiora, John Langford, and Michael L Littman. Pac model-free reinforcement learning. In *Proceedings of the 23rd international conference on Machine learning*, pages 881–888. ACM, 2006.

Takuya Sugimoto and Manabu Gouko. Acquisition of hovering by actual uav using reinforcement learning. In *Information Science and Control Engineering (ICISCE), 2016 3rd International Conference on*, pages 148–152. IEEE, 2016.

Richard S Sutton and Andrew G Barto. Reinforcement learning: An introduction, 1998.

Matthew E Taylor, Peter Stone, and Yaxin Liu. Transfer learning via inter-task mappings for temporal difference learning. *Journal of Machine Learning Research*, 8(Sep):2125–2167, 2007.

Pratap Rajkumar Tokekar. *Placement and Motion Planning Algorithms for Robotic Sensing Systems*. PhD thesis, Citeseer, 2014.

Christopher JCH Watkins and Peter Dayan. Q-learning. *Machine learning*, 8(3-4):279–292, 1992.

Marco Wiering and Martijn Van Otterlo. Reinforcement learning. *Adaptation, Learning, and Optimization*, 12, 2012.